ZRNIC

SPECTRUM WIDTH STATISTICS
OF
VARIOUS WEATHER PHENOMENA

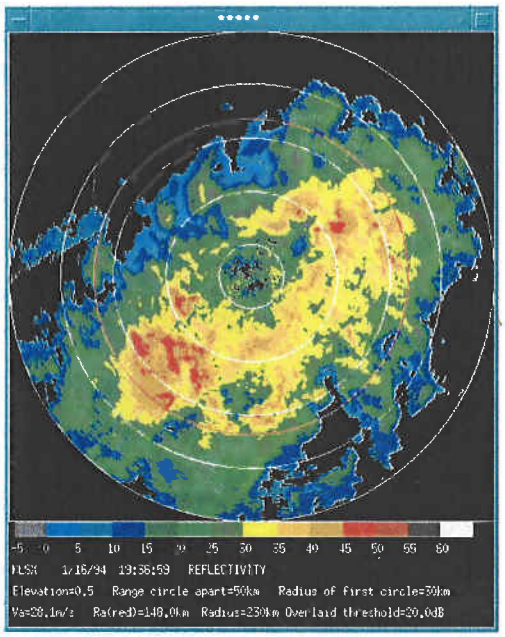

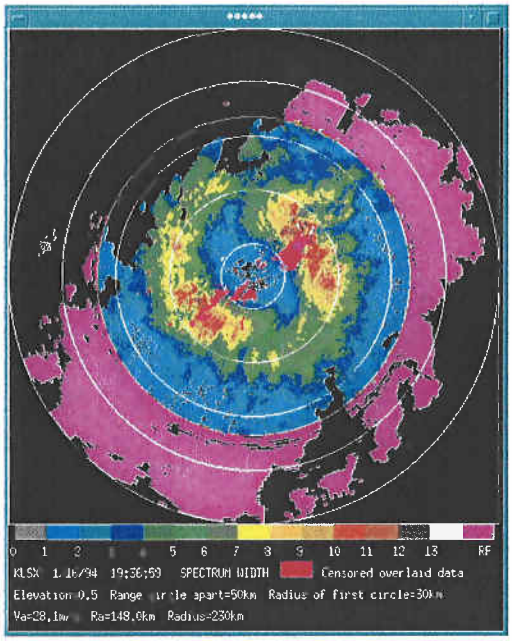

Ming Fang
Cooperative Institute of Mesoscale Meteorological Studies
Richard J. Doviak
National Severe Storms Laboratory
1313 Halley Circle
Norman, Oklahoma 73069

September 2001

TABLE OF CONTENTS

Cover pictures depict the reflectivity and spectrum width fields measured by a WSR-88D radar observing a snow storm over St. Louis Mo. The enhanced semicircles of spectrum width suggest a shear layer at an altitude of about 1 km AGL. See section 3.7 for more discussion.

1. Introduction

This study is motivated by the fact that spectrum width, σ_v, has the potential to improve the interpretation of weather radar data which can lead to better warnings of severe weather (Lemon, 1999) and hazards to safe flight (Mahapatra, 1999). Turbulence, a hazard to safe flight, is a main contributor to spectrum width (Istok and Doviak, 1986), and spectrum width remains the principal means to detect regions dangerous for safe flight (Cornman, et al., 1999). However, the use of spectrum width data has been very limited, at least compared to that of the reflectivity and Doppler velocity fields. This is due in part to the difficulty in relating σ_v to meteorologically significant phenomena (e.g., turbulence hazards to safe flight), and in part to the fact that σ_v values are easily corrupted by radar artifacts (e.g., improper AGC settings, Signal-to-Noise Ratio, SNR, thresholds set too low, etc.) which make the spectrum widths unreliable and more risky to interpret.

Another motivation for this study is that the capabilities of a Doppler weather radar to resolve range and velocity ambiguities strongly depends on the width σ_v of the Doppler spectrum. WSR-88D specifications are based on analysis of data from research radars which showed that the median value of spectrum width in tornadic storms was about 4 m s^{-1} (Doviak and Zrnic, 1993, p.412). Also, theoretical studies on methods to mitigate the effects of ambiguities typically assume spectrum width values of about 4 m s^{-1}. But this median value is derived from only three storms; furthermore, tornadic storms comprise a small percentage of the weather being observed with Doppler radars. There are several approaches to mitigate the effects of ambiguities in Doppler radar data (Doviak and Zrnic, 1993, Section 7.4), but they all require signal samples be well correlated. The coherency condition (Doviak and Zrnic, 1993, section 7.3),

$$\sigma_v \le \frac{v_a}{\pi} \tag{1}$$

where $v_a = \lambda/4T_s$, λ is the radar wavelength, and T_s is the pulse repetition time (i.e., the PRT), insures that signal samples are correlated. As a matter of fact, overlaid weather signals can be perfectly separated, and spectral moments of each of the overlaid signals can be unambiguously estimated if σ_v is sufficiently small (Sachidananda and Zrnic, 1999).

Sachidananda (1998) developed a family of systematic phase codes (i.e., the SZ codes) which, when used to modulate the phase of the transmitted signal, allows separation of overlaid weather signals. But the performance of these codes strongly depends on the widths of the overlaid Doppler spectra; if spectrum widths exceed about 1/5 of v_a, the performance of the algorithms rapidly deteriorate. For example, it has been shown by Sachidananda (1998, e.g., Fig. 3.16) that there is a significant increase in the variance of the velocity and spectrum width estimates when σ_v exceeds about 5 m s^{-1} for the PRTs typically used by the WSR-88D (i.e., 21 < v_a < 32 m s^{-1}). For example, velocity standard error more than doubles that obtained if the SZ(8/64) phase coded algorithm is used to separate overlaid echoes and σ_v is 7 m s^{1}. Similar increases in velocity standard error are found if a staggered PRT method is used to extend the unambiguous velocity v_a and/or unambiguous range r_a (Sachidananda, 1999, e.g., Fig. 3.5).

Although these methods improve the performance of the radar, the level of improvement depends on σ_v and, in turn, these depend on the type of weather being observed.

The algorithms required to process the SZ coded echoes are computationally intense, and require extensive modification of the existing hardware for the WSR-88D. Planned upgrades to the WSR-88D (Zahrai, et al., 1998) will allow implementation of these algorithms. Thus, one of the aims of classifying spectrum widths according to the type of weather and as a function of range and elevation angles (to be investigated in the next period), is to estimate the expected improvement in the performance of upgraded Doppler weather radars that might utilize these newly developed codes. Thus, in this report we compute the probability distribution (and the cumulative probability) of σ_v measured with the 10-cm wavelength WSR-88D in the volume of space occupied by various classes of weather defined in Section 3. We summarize these statistics by tabulating the median value of σ_v for various classes of weather and the per cent of widths larger than 8 m s^{-1} (this is about the upper limit of σ_v for which overlaid spectra can be separated using the SZ algorithms of Sachidananda, 1998).

2. Error sources for spectrum widths observed with the WSR-88D

In this study we use WSR-88D data because its widespread availability provides us with many opportunities to obtain a wide variety of weather types for analysis, and because the WSR-88D data is more amenable to editing of erroneous data. It is well known that estimates of σ_v, the square root of the second central moment of Doppler spectra, are more prone to errors than the zeroth (power, or reflectivity) or the first (i.e., mean Doppler velocity) moments. For example, the estimates of reflectivity observed with the WSR-88D always use sufficiently long PRTs so that there are no reflectivity errors due to overlaid echoes. On the other hand the Doppler velocity v and spectrum width σ_v must be estimated using relatively short PRTs which often leads to conditions of overlaid weather signals that can corrupt the v and σ_v measurements.

2.1 *Errors due to overlaid echoes*

If the in-trip echo power is more than $T_0 = 20$ dB stronger than the *sum* of out-of-trip echo powers (T_0 is the overlaid threshold), it can be shown that the spectral moments of the stronger signal can be estimated without significant error (i.e., the NEXRAD Technical Requirements, Table 1, are still met). The 20 dB overlaid threshold would censor Doppler velocity v and spectrum width σ_v data for which the echo power (used in computing the reflectivity field) from scatterers at an in-trip range is less than 20 dB above the *sum* of echo powers from the out-of-trip ranges; this threshold insures that both v and σ_v measurements met specifications. Nevertheless, v estimates can still meet specifications with a much lower overlaid signal threshold (e.g., $T_0 = 10$ dB).

Table 1
NEXRAD Technical Requirements (1991) for estimate accuracies

Conditions:
True spectrum width = 4 m s^{-1}
For velocity estimates the Signal to Noise Ratio is: SNR ≥ 8 dB;
For reflectivity factor and spectrum width estimates: SNR ≥ 10 dB
Standard errors include quantization errors. Angular resolution = 1°.

parameter	standard error	quantization interval	range resolution
reflectivity factor, Z'	1 dB	1 dB	1000 m
radial velocity, v	≤1.0 m s^{-1}	0.5 m s^{-1}	250 m
spectrum width, σ_v	≤1.0 m s^{-1}	0.5 m s^{-1}	250 m

[1]Note, because long PRTs are used when Z is estimated, there is little chance that there are errors in Z due to overlaid echoes.

The overlaid threshold test in the WSR-88D compares the in-trip echo power, in each one kilometer range averaging-interval range Δr = 1 km (Doviak and Zrnic, 1993, Section 6.3.2), obtained using long PRTs (either in separate azimuth surveillance scans separated by about 20 seconds, or on separate data radials separated about 0.5°), with the significant signal power in *each* of the out-of-trip Δr that would overlay the in-trip echoes. That is, the summed out-of-trip echo power is *not* used. Significant signal power, obtained during the long PRT or Surveillance periods, is that which exceeds a signal threshold T_{sS}. Since about 1996 this has been set at T_{sS} = 2.0 dB (i.e., the signal-to-noise power ratio, SNR = 2.0 dB). During the Doppler data collection mode (i.e., data collected using short PRTs), echo power (called the "Doppler" echo power) is also computed and compared with another signal threshold T_{sD}. But "Doppler" echo power is the sum of echo powers from each of the trips. An additional signal power test is applied to determine whether to censor velocity data based on SNR when data is collected in the Doppler mode. In this signal power test, the summed echo powers must exceed a Doppler signal power threshold T_{sD}. = 3.5 dB. If the in-trip echo power passes the T_{sS} and T_{sD} SNR tests, then the overlaid echo power test is made on the data collected during the surveillance scan. For the in-trip velocity and spectrum width estimates to pass the overlaid test, the in-trip echo power must exceed the power in *each* of the corresponding out-of-trip regions by a threshold T_o'. Since about 1996 the overlaid test has been that the in-trip echo power must exceed by 5 dB (i.e., T_o' = 5 dB) the significant echo power calculated from data collected in the surveillance mode for each corresponding Δr in the out-of-trip regions.

In this report, however, the overlaid threshold T_o is that level or larger above the *sum* of out-of-trip echo powers that the in-trip echo power must achieve in order to declare that the velocity and spectrum width estimates are valid. Comparing the in-trip echo power with the sums of the out-of-trip powers is a more demanding criterion than comparing the powers individually from each out-of-trip region.

The overlaid signal threshold in the WSR-88D cannot be set separately for the velocity and spectrum width estimates. However, future upgrades to the WSR-88D (Zahari et al., 1998) will allow separate settings. For now, and because most radar meteorologists are interested in the Doppler velocity v fields and not the spectrum width σ_v fields, the above specified low overlaid signal threshold T_o' = 5 dB is used for both v and σ_v. With T_o' = 5 dB, the velocity estimates can have errors that exceed those specified for non overlaid echoes (i.e., ≤ 1 m s^{-1}). Nevertheless, for the interpretation of the Doppler velocity fields on weather radar displays, this increase in velocity estimate errors is not noticeable, principally because it is masked by the quantization intervals used to display Doppler velocity fields. But the 5 dB overlaid threshold plays havoc for reliable spectrum width estimation.

For example, the percent of spectrum width values exceeding 8 m s^{-1} for spectrum width data collected on a squall line that passed through St. Louis MO, on the 15th of April, 1994, decreased from 10.7% when a T_o = 10 dB overlaid threshold was used, to 9.8% when a 20 dB threshold was used. The percentage of spectrum widths exceeding 8 m s^{-1} was even larger when the WSR-88D default threshold value T_o' = 5 dB was used. For the three tornadic storms studied

herein, spectrum width values exceeding 8 m s^{-1} was less than 1% when the 20 dB threshold was applied compared to about 10% for the tornadic storm data presented by Doviak and Zrnic (1993) in which overlaid echoes were assumed not to be present. Thus, to have acceptable σ_v estimates, an overlaid threshold of 20 dB is hence forth used for the data presented in this report. It is important to note that we can apply, to recorded WSR-88D data, values for T_o higher than 5 dB because we have unambiguous reflectivity data from which we can compute echo powers. Because we did not have calibration data for each of the data sets analyzed, we estimated the relative signal power in each of the trips; it is the relative signal power that is important in censoring overlaid echoes.

An example of spectrum width estimates being corrupted by overlaid echoes is in Figs. 1. Fig. 1a shows the reflectivity field of stratiform precipitation with embedded weak convective elements observed with the WSR-88D in Des Moines, Iowa, on 05/27/1995. The 460 km x 460 km square box in Fig. 1a encloses all the available Doppler data presented in Figs.1b to 1d. Because Doppler velocities are not the focus of our study, they are not presented unless there is a relation between the width and velocity fields that helps in the meteorological interpretation of the σ_v data. On the other hand, reflectivity factor fields will be consistently shown because they are helpful in identifying anomalies likely to cause errors in the interpretation of data. Such errors are likely to occur in regions where weather signal power is weak and *SNR* small. Reflectivity data are also helpful in classifying weather, and, as well, suggest where overlaid echo powers could be troublesome.

In Fig. 1b shows the Doppler velocity v field, wherein the "S" pattern of isodops suggest that wind veers with height. Veering is deduced because more distant data are also from higher altitudes, and if wind is vertically stratified the range dependence translates to a height dependence. The important point, however, is that because wind is veering with height, second trip velocities from higher altitudes are likely to be different than first trip ones. Thus the effects of overlaid echoes on spectrum width estimates will be more pronounced. Fig. 1c presents the associated spectrum width field. All reflectivity data are estimated during surveillance scans using long PRTs (i.e., T_s) which practically precludes overlaid echoes. But velocity and spectrum width are not estimated during these surveillance scans because the coherency condition (1) is often violated, and velocity ambiguities are prevalent (e.g., at elevation angles of 0.5° and 1.5° the unambiguous velocity $v_a = \lambda/4T_s$ is about 8 m s^{-1} during the surveillance scans).

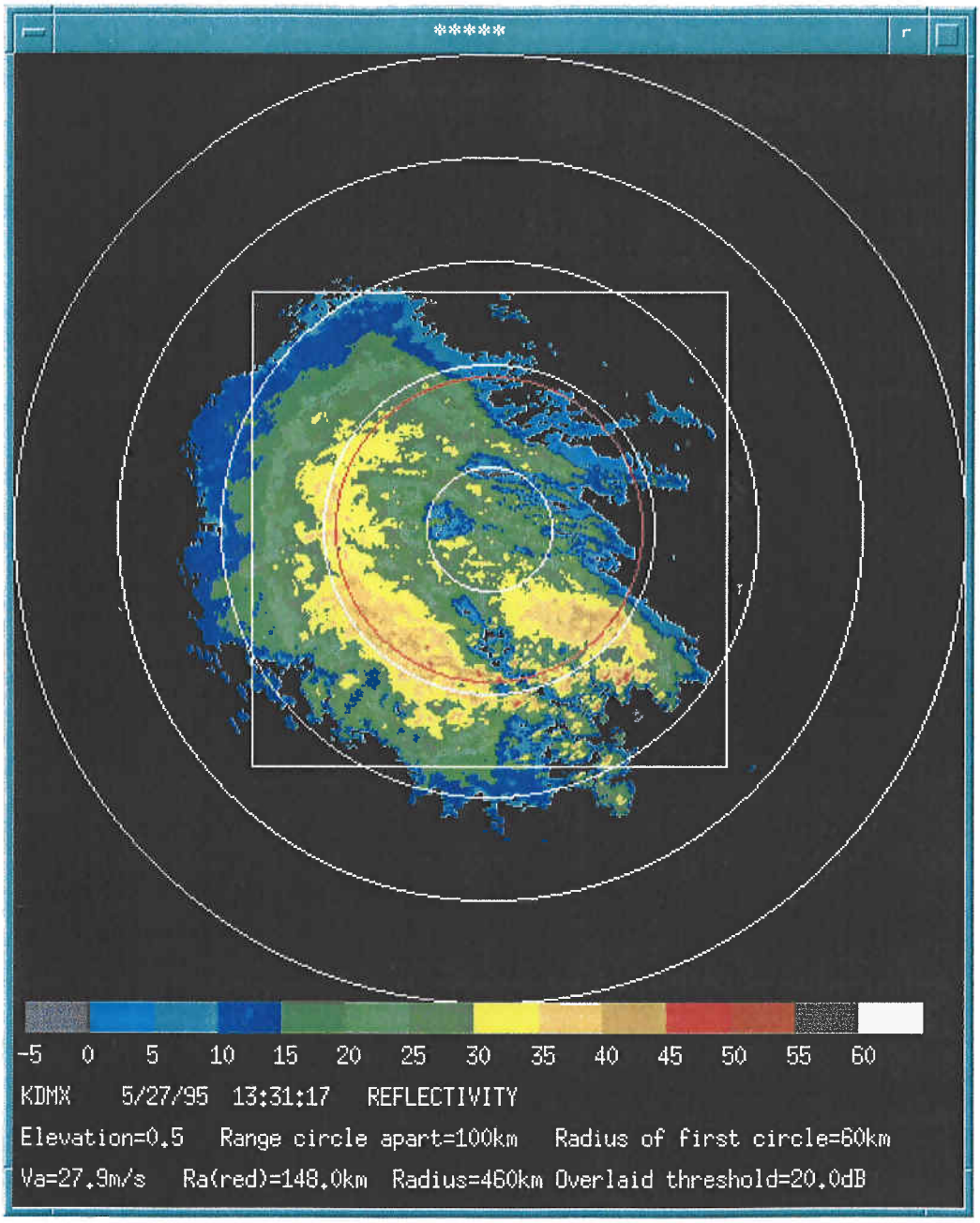

Fig.1a The Reflectivity Factor field observed by the KDMX WSR-88D in Des Moines, IA during large scale showers. The white square outlines the area shown in Figs. 1b, 1c. The color scale is Reflectivity Factor in dBZ. The red circle locates the unambiguous range (148 km) when Doppler data are collected (Figs. 1b, 1c).

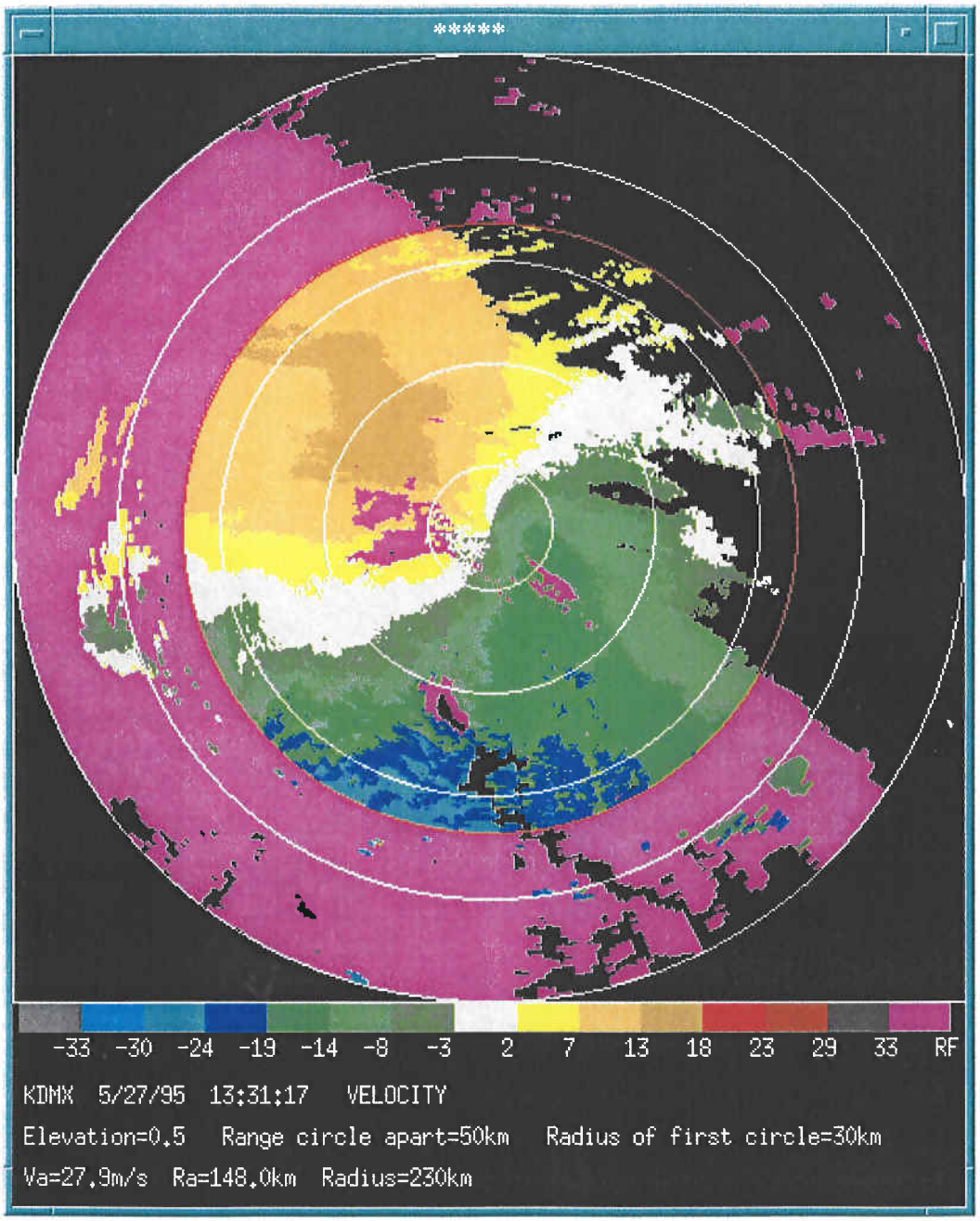

Fig. 1b The Doppler velocity field associated with Fig. 1a. The color bars designate Doppler velocity in m s^{-1}. A 5 dB overlaid threshold was applied to the data and the purple shaded areas are those regions where power from out-of-trip echoes is -5 dB or larger than the in-trip echo power.

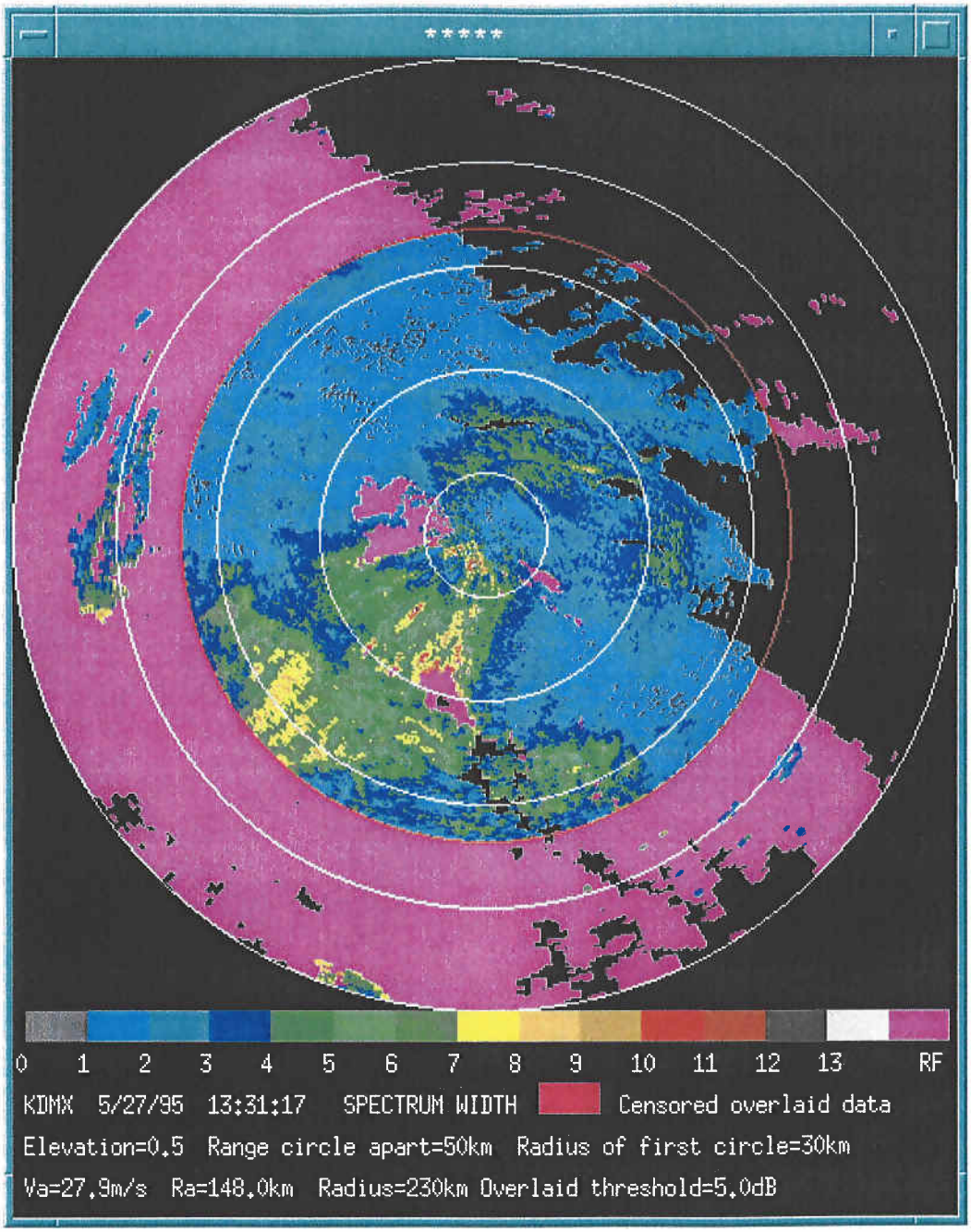

Fig. 1c The spectrum width field with a 5 dB overlaid threshold. The color bar designates width values in m s^{-1}.

Correcting aliased velocities is difficult if they are inaccurate and aliased multiple times. Hence velocity and spectrum widths are calculated during separate scans about 20 seconds later at the same elevation angles using short PRTs for the 0.5° and 1.5° elevation cuts. But this results in shorter r_a and a large occurrence of overlaid echoes. The red circles in Figs. 1 define the unambiguous range when the Doppler velocity and spectrum width are calculated. The data presented in Figs. 1b (Doppler velocity) and 1c (spectrum width) were censored using an overlaid threshold T_o = 5 dB (typical of that used in the WSR-88D network since 1996). Regions of large spectrum widths (the yellow colored areas), at ranges between 55 and 83 km to the southwest, appear to be anomalously large. Because the 5 dB overlaid threshold has censored σ_v cores of these cell-like regions, it is concluded that second trip reflectivity fields, with echo powers stronger than the first trip ones by at least -5 dB, are overlaying the first trip ones. The high σ_v values surrounding these cell like structures are also likely corrupted. Using the larger overlaid threshold T_o = 20 dB (Fig.1d) these areas of suspiciously high σ_v are censored. Furthermore, some areas of large spectrum widths (the blue region; σ_v = 3 to 4 m s^{-1}) to the west between 80 and 110 km are censored. These regions might also have spectrum width estimates that are biased high by overlaid echoes.

But not all regions of overlaid echoes necessarily have corrupted σ_v values, even if they met the criterion for censoring. For example, if the Doppler spectra of two overlaid echoes have the same mean velocity and spectrum widths, the estimated width will be correct for both regions. Nevertheless, although censoring data based on power ratios might cause the loss of some valid data, the resulting data fields are guaranteed to have valid σ_v. For example, by comparing Fig.1c with Fig.1d, we see that most of the data lost occur in regions where spectrum width values are large. Thus we allow the sacrifice of some valid spectrum width data to insure that the analyzed data are free from errors due to overlaid echoes.

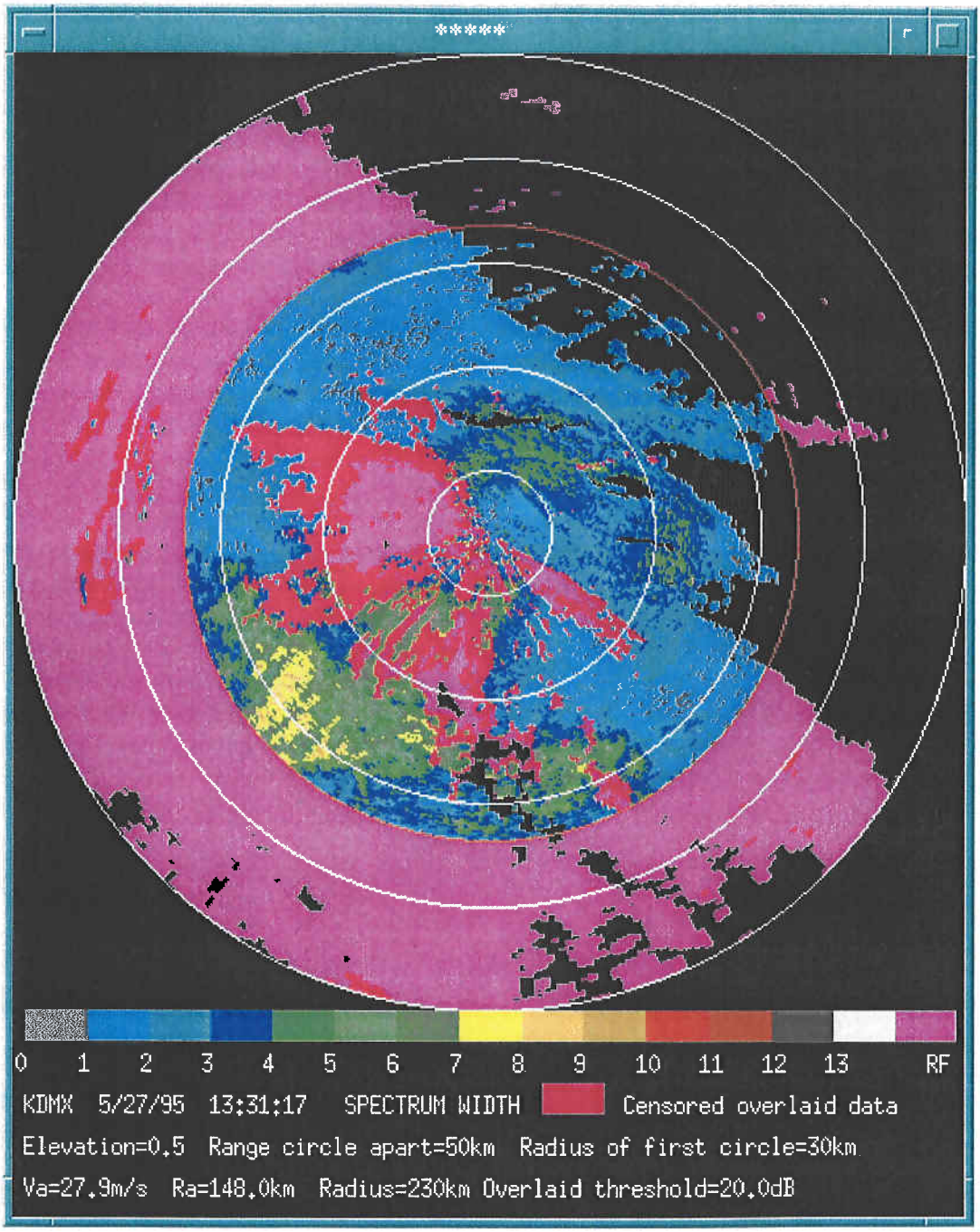

Fig. 1d The same spectrum width field as in Fig.1c, but the overlaid threshold is 20 dB.

2.2 *Errors due to low signal-to-noise ratios*

Besides spectrum width estimates being corrupted by overlaid echoes, the spectrum width estimates are more prone to errors due to receiver noise, and to incorrect estimates $\overline{N}$ of receiver noise power N, than are velocity estimates. The WSR-88D hardware calculates the autocovariance at lags 0 and 1 to estimate spectrum widths using the PPL formula

$$\hat{\sigma}_v = \frac{v_a}{\pi}\left|\ln\left(\frac{\hat{S}^2}{|\hat{R}^2(T)|}\right)\right|^{1/2} sgn\left[\ln\left(\frac{\hat{S}}{|\hat{R}(T)|}\right)\right] \tag{2a}$$

given by Doviak and Zrnic (1993; Eq.6.27), where $\hat{S}$ is the estimate of signal power

$$\hat{S} = \frac{1}{M}\sum_{k=0}^{M-1} |V(k)|^2 - \overline{N}\,. \tag{2b}$$

$V(k)$ is the kth sample of signal plus noise, T is the PRT during the Doppler data collection mode, M is the number of samples used in estimating S and $R(T)$, and $\overline{N}$ is noise power measured during the calibration of the radar. As explained later in this section, the *sgn* function is used to flag spectrum widths for which the argument of the logarithmic function is less than one.

An overline on N is used to differentiate this estimate, which uses many more samples than that M, from estimates which use M samples. Noise calibration takes place during the elevation angle retrace period after every volume scan while the transmitter is shut off. Because the estimate $\overline{N}$ is an average of noise power over many more than M samples, the statistical errors should be minimal. On the other hand, the noise power is a function of beam direction; more noise power is encountered at low elevation angles when part or all of the beam intersects the warm earth, or when the beam is pointed at relatively warm precipitation. With high performance radars having low noise microwave receivers, such as the WSR-88D, the changes in noise power can be as much as a dB.[2] Thus the noise power $\overline{N}$ made during the calibration can differ from N when data is being collected and adjustments are required to account for these differences; these adjustments are not made by the WSR-88D signal processors during routine data collection, nor is it, to the authors' knowledge, made in any research Doppler radar. In the following paragraphs it will be shown the bias in noise power as small as 0.5 dB can cause biases larger than 0.5 m s^{-1} in spectrum width estimates if SNR is less than about 20 dB.

In addition to biases, the variance of spectrum width estimates become unacceptably large when too low a SNR threshold is used. For example, in order to display larger areas of Doppler velocity in weak reflectivity regions, the WSR-88D radars employ (since 1996) a SNR threshold

---

[2]This is based on measurements, made by Dr. Valery Melnikov, of NSSL's R&D WSR-88D noise power. These measurements showed about a 0.7 dB increase in receiver noise temperature if the radar beam is directed, at high elevation angles, at the relatively cold clear sky, and then is directed towards the warm earth.

T_{sD} = 3.5 dB, instead of the design threshold of 10 dB (an example of the increase in the variance of spectrum width estimates will be presented in the next section). Although this threshold is lower than required to meet the design specifications for velocity errors (i.e., ≤ 1.0 m s^{-1}), the increase in error is modest. For example, if the spectrum width is 5 m s^{-1}, and v_a = 25 m s^{-1}, the standard error of $\hat{v}$ is about 1.1 m s^{-1}. Although SNR thresholds can be independently set for the three spectral moments, the same 3.5 dB threshold is used for spectrum width. If this threshold is also used for spectrum width estimation, a standard error of 1.4 m s^{-1} is generated (i.e., the variance of the estimate is doubled!).

Furthermore, it should be noted that if the true noise power N is overestimated with a measured value $\overline{N}$, the PPL algorithm could have the argument of the logarithm persistently less than one, especially if S/R(T) = $\{R(0) - N\}/R(T)$ is near 1 as expected for small spectrum widths; this holds for any SNR. Under this condition the width estimates would be imaginary; the absolute sign in Eq.(2a) is used to avoid imaginary widths. If true spectrum widths are small, imaginary width occurrences can also be caused by statistical fluctuations in the estimates of signal power; again, even if SNR = ∞. If the argument of the logarithmic function in Eq.(2) is less than one, the signal processors in the WSR-88D set $\hat{\sigma}_v$ to zero. The purpose of the *sgn* function in Eq.(2a) is to identify these imaginary width values and to assign a zero value to them. If N is overestimated ($\overline{N} > N$), and true spectrum widths are small, spectrum width estimates will be biased and an excessive occurrence of zero or imaginary width assignments will be made (Melnikov and Doviak, 2001). For the statistical analysis presented herein, these zero values are ignored.

To further illustrate the noise measurement problem, it can be shown that, under operating conditions typical of weather radars where N/S << 1, the maximum bias, $\Delta_{\mp}\sigma_v$, in the spectrum width estimate $\hat{\sigma}_v$ due to incorrect measurements of noise power is (Melnikov and Doviak, 2001)

$$Max[\Delta_{\mp}\sigma_v] \equiv Max[\hat{\sigma}_v - \sigma_v] \approx \frac{v_a}{\pi}\sqrt{\frac{N}{S}\left|\frac{\epsilon_{\pm}(dB)}{2.17}\right|} \qquad (3)$$

where $\epsilon_{\pm}$ is the dB error in noise power measurements, v_a is the unambiguous Doppler velocity, and σ_v is the true spectrum width. Bias is a function of true spectrum width, and there is a very different dependence of the bias if noise power is overestimated versus what it would be if noise power is underestimated; the above equation only gives the maximum bias. The bias is negative (i.e., σ_v is underestimated) if the noise power is overestimated (i.e., ϵ(dB) = ϵ_+(dB) > 0) and positive if noise power is underestimated. If ϵ(dB) is negative, the maximum positive bias given by Eq.(3) occurs when true width approaches zero, but if ϵ(dB) is positive, the maximum underestimate of σ_v occurs at $\sigma_v = Max[\Delta_- \sigma_v]$. Thus, if there is a 0.5 dB difference between $\overline{N}$ and N, a SNR(dB) of about 20 dB (for v_a of about 30 m s^{-1}) is required to insure that biases are less than 0.5 m s^{-1}. Under the condition SNR = 20 dB, and if noise power is overestimated, the maximum bias occurs at a true spectrum width of 0.5 m s^{-1}; if noise is underestimated by 0.5 dB, the maximum bias occurs at σ_v = 0. Such large SNR thresholds are rarely used to censor data.

For example, the threshold on SNR in the USA's network of weather radars, is typically set at about 3.5 dB, and hence it can be expected that significant biases can occur if noise power is not precisely measured.

To mitigate errors due to low *SNR* if $\overline{N} \neq N$, a relatively large *SNR* threshold (i.e., 20 dB) is employed when analyzing spectrum width data. The WSR-88D default SNR and overlaid thresholds are used when presenting the velocity and reflectivity displays.

2.3 *Errors due to improper AGC settings*

The incorrect setup of the Automatic Gain Control (AGC) circuits is another source of error in spectrum width estimates. If the AGC is properly setup, signal levels will never be so strong that they exceed the maximum level of the analog-to-digital converter (ADC). If weather signals exceed this level, the signals are clipped and harmonics of the weather spectrum are generated. These harmonics increase the estimated spectrum width values.

Examination of spectrum width data at many radar sites showed that the unusually significant correlation of large spectrum widths with large echo powers can be due to improper setup of the AGC (Sirmans, et al., 1997). Fig.2 shows the displays of (a) reflectivity, (b) Doppler velocities, and (c) spectrum widths obtained from the KFSD, WSR-88D radar on 05/31/98. The areas of purple in Fig. 2b represent censored data for which the overlaid threshold T_o' is not exceeded (i.e., the signal power at the selected trip range does not exceed the assigned threshold value; in this case $T_o' = 5$ dB above *each* of the significant out-of-trip echo powers) which is the areas censored by the WSR-88D algorithms; that is, we have not increased the censoring threshold. The areas of bright red-purple in Fig. 2c represent censored data for which the overlaid threshold T_o is not exceeded (i.e., the signal power at the selected trip range does not exceed the assigned threshold value; in this case $T_o = 20$ dB above the *sum* of the significant out-of-trip echo powers); that is, we have increased the overlaid censoring threshold for the spectrum width data fields.

The SNR thresholds used to produce Fig. 2a is $T_{sS} = 2.0$ dB, and to produce Figs. 2b and 2c the SNR threshold is $T_{sD} = 3.5$ dB, the values routinely used by the WSR-88D. Henceforth, the overlaid threshold for the Doppler velocity field and SNR thresholds for the reflectivity field and Doppler velocity are those imposed by the WSR-88D; that is, there is no further censoring of these data fields. However, for the spectrum width field presented in Fig. 2c the bright red-purple and purple areas represent censored data based on an overlaid threshold value $T_o = 20$ dB that has been imposed on the data fields; the in-trip echo power must exceed the *sum* of out-of-trip echo powers by 20 dB in order for spectrum estimates to be considered valid.

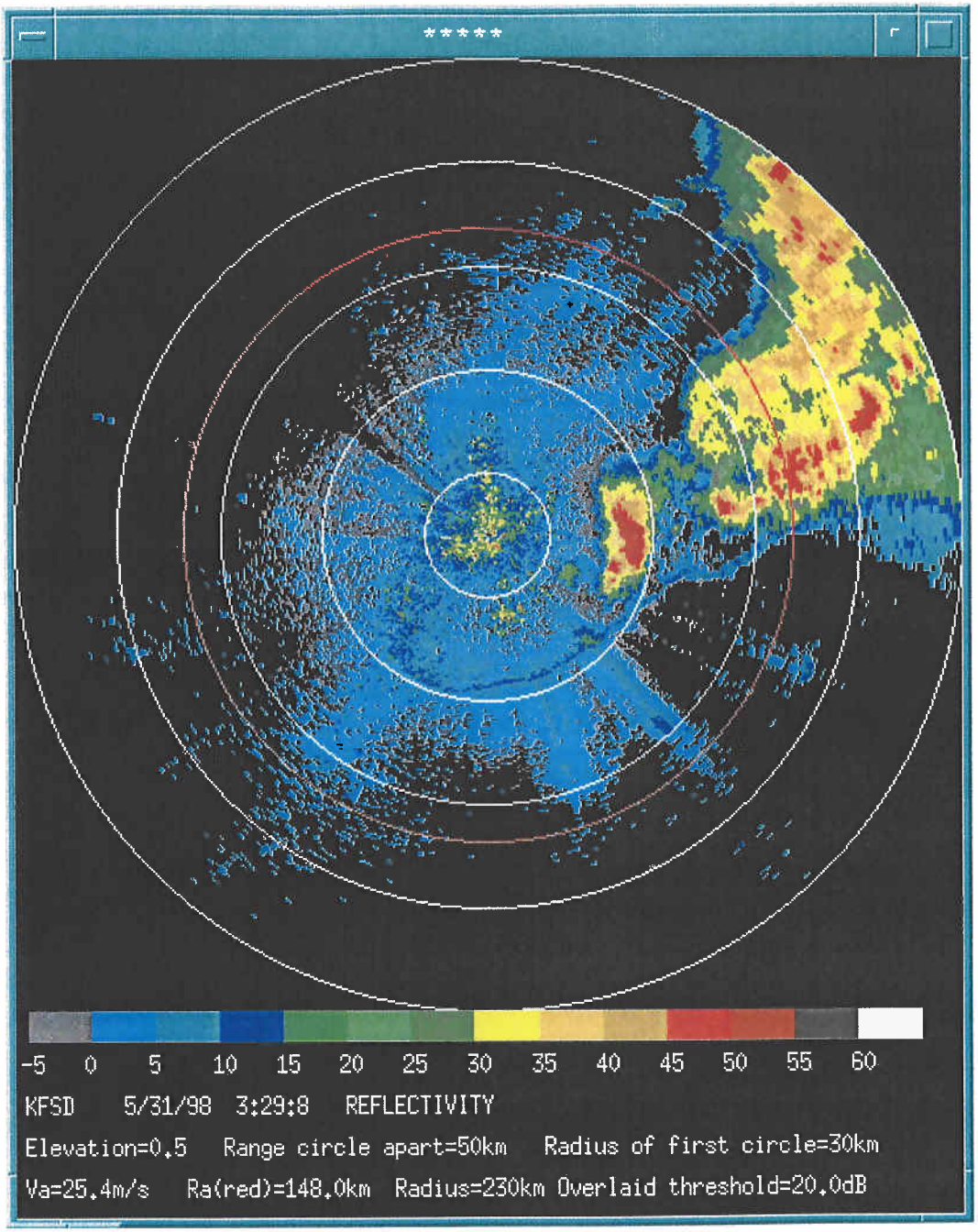

Fig. 2a) The Reflectivity Factor field showing strong reflectivities to the east of the radar site which over drive the AGC circuits and bias spectrum width estimates (Fig. 2c).

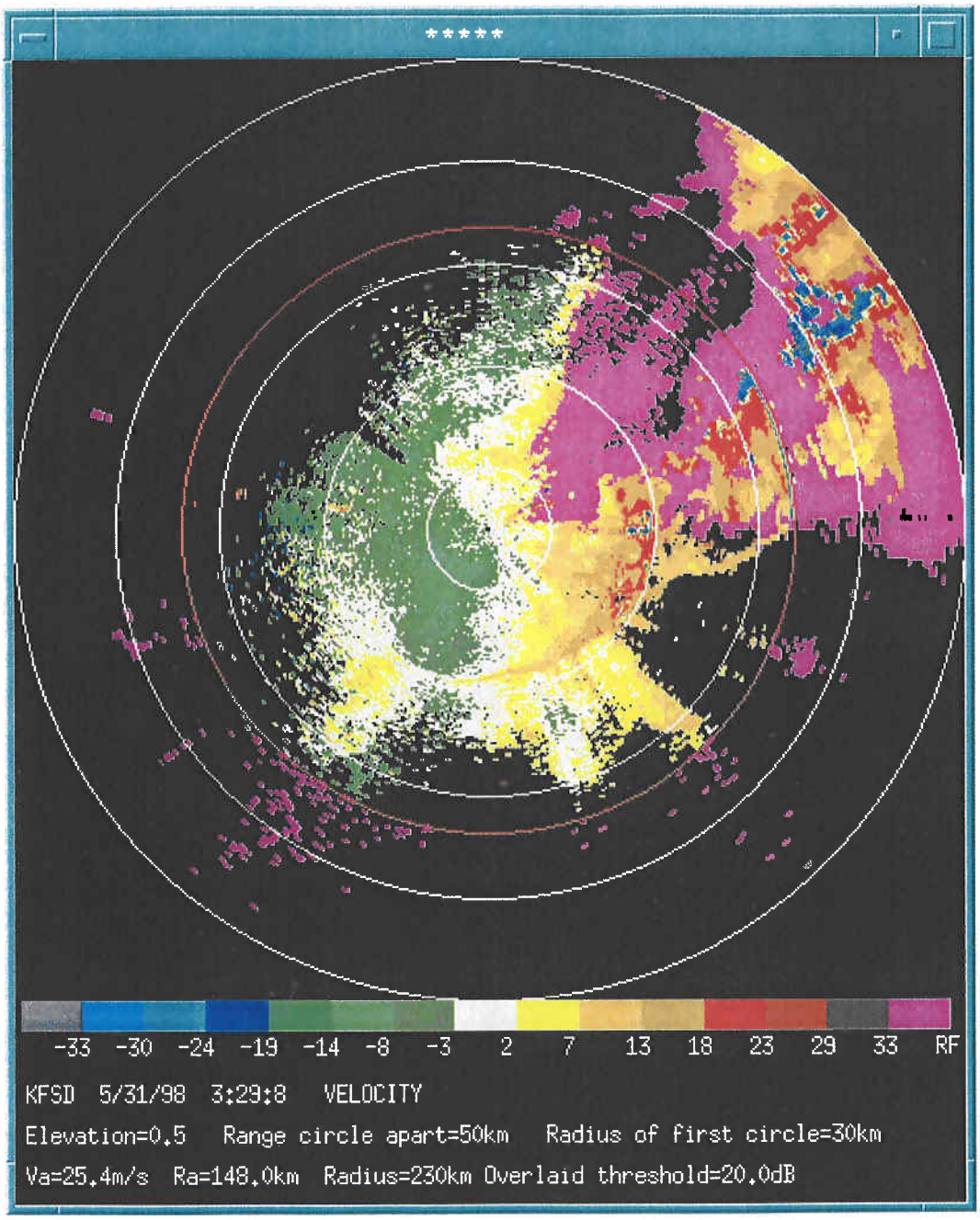

Fig. 2b) The Doppler velocity field associated with Fig. 2a. The overlaid threshold is set to 20 dB (5 dB is routinely used) and the SNR threshold is that 3.5 dB used for the WSR-88D radars. The enhanced velocities along the gust front south and southeast of the radar marks the leading edge of denser air outflow from the thunderstorms which are propagating eastward.

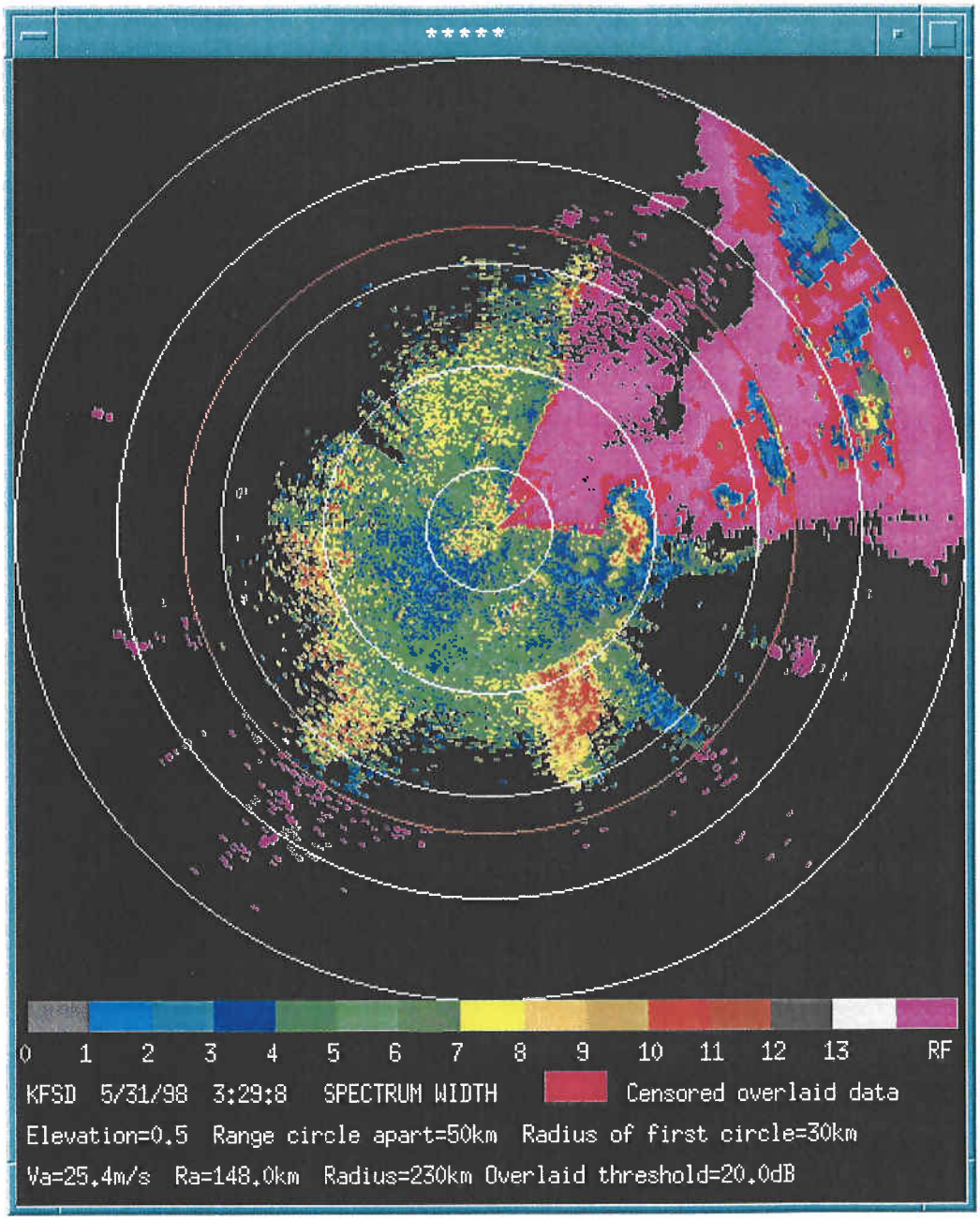

Fig. 2c) The spectrum width field associated with Fig. 2b. Note the region of enhanced spectrum width, to the east at about 70 km, which is highly correlated with the region of high reflectivity. This is due to over-driven AGC circuits. The large and noisy spectrum width estimates *at ranges beyond 80 km and to the west and South of Southwest are likely due to low SNR. The SNR threshold is 3.5 dB.*

The area of high reflectivity values exceeding 40 dBZ to the east of the radar (Fig. 2a) at a range of about 70 km are positively correlated with high spectrum width values exceeding 7 m s^{-1} (Fig. 2c). But the equally high reflectivity area a bit north of east at about twice the range has much smaller width values showing that the correlation is with power not reflectivity; the decrease of power by 6 dB due the more distant range of that reflectivity area is sufficient to noticeably diminish the high values of spectrum widths. Nevertheless, the spectrum widths in this region could still be biased marginally high because the ADC might still be clipping the stronger portions of a fluctuating weather signal, although not to the extent of those echoes from the high reflectivity area closer to the radar. Furthermore, the high reflectivity region to the east of northeast at a range of about 200 km has associated with it high spectrum widths. But because the reflectivity in this region is not significantly larger than that at140 km, it is unlikely these are caused by an over driven AGC; therefore these widths should be valid.

Also notice in Fig. 2c the area of large spectrum widths with considerable spatial variability to the west and southwest at ranges from about 90 to 230 km. This is an area of weak reflectivity and thus spectrum width estimates could have excessive spatial variance because of low SNR. Furthermore, these estimates could be biased by incorrect measurements $\overline{N}$ that estimate the noise power N. Note that the spectrum widths appear to be biased high which implies, using Eq.(3), that the noise power is underestimated (i.e., biased low). Thus, noise power measurements made at high elevation angles appear to underestimate the noise power when the beam is directed at 0.5°. In Fig. 2d the SNR threshold T_{sD} has been increased 15 dB, and it is seen that these areas of large spectrum width with considerable spatial variance have been, for the most part, censored.

The area of spectrum widths larger than 7 m s^{-1} to the southeast at ranges beyond 75 km is due to ground clutter made visible through anomalous propagation conditions, as well as too low a SNR. Note in Fig. 2b the abundance of zero and anomalously small Doppler velocities. The anomalous propagation condition is likely due to the cold air outflow from the thunderstorms which produce a strong ground based temperature inversion that bends the radar beam toward the earth (Doviak and Zrnic, 1993, Section 2.2.3.2); the leading edge of this outflow is marked by the arc of enhanced reflectivity factors seen in Fig. 2a, as well as by the arc of enhanced Doppler velocities (Fig. 2b) at a range of about 75 km southeast of the radar. Thus the spectrum widths in this region are not representative of velocity variance within the radar's resolution volumes, and they must be edited by other means that, except for the deductive reasoning just described, are beyond the scope of this work.

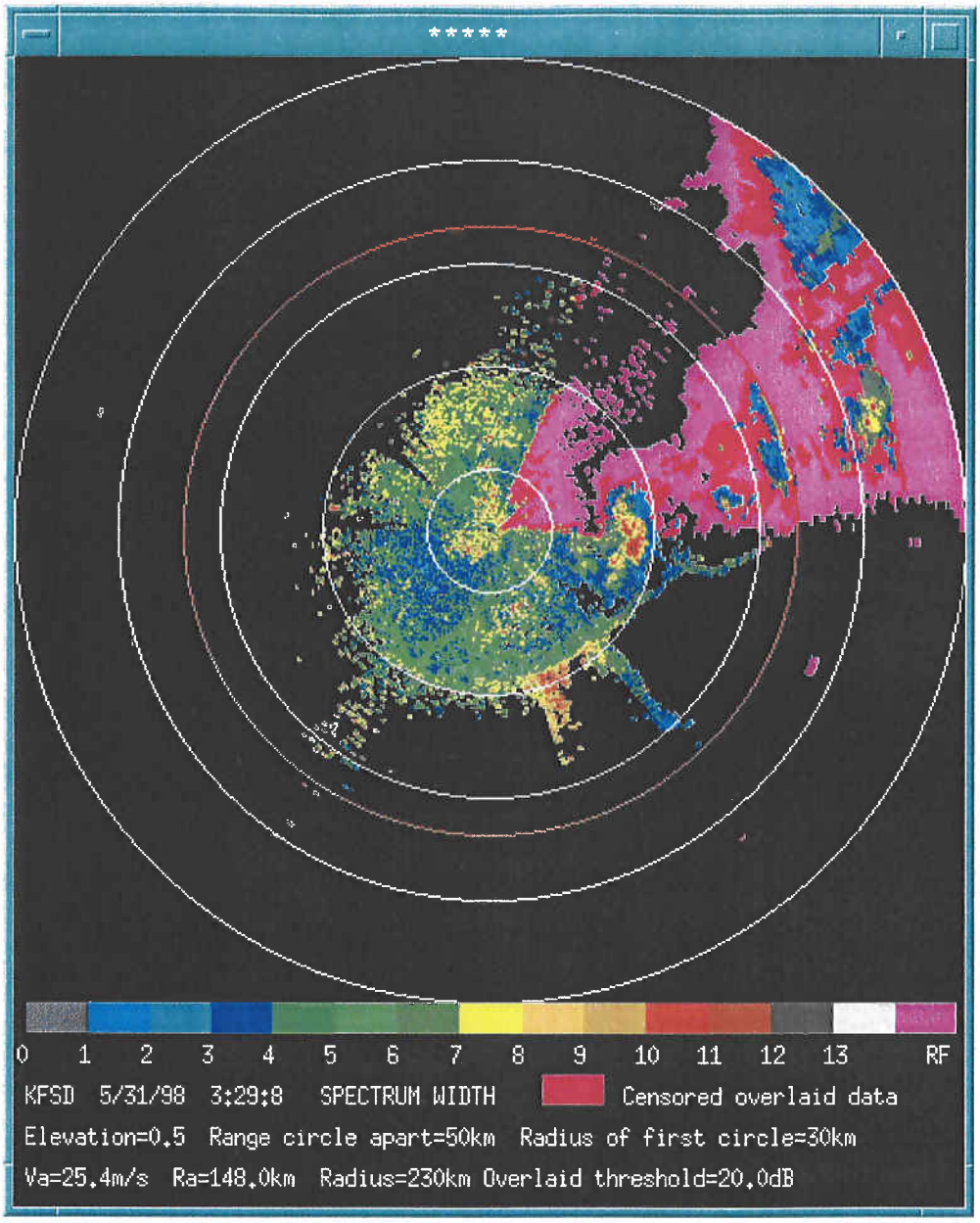

Fig. 2d The spectrum width field as in Fig. 2c, but the SNR threshold has been increased to 15 dB. Note that high spectrum width values with high spatial variance in the region from the west to south of SW have been censored. These high values with high spatial variability are likely due to low SNR and/or improper estimates of noise power.

2.4 *Editing procedures applied to censor potentially erroneous spectrum width data*

In order to have reliable spectrum width values for classification, spectrum values cannot be used as is without editing the data for the previously mentioned anomalies. By far the most persistent anomalies appear to be those due to overlaid signals, and noise power. Thus algorithms have been developed to objectively select data which have a signal power level at least 20 dB higher that the sum of competing out-of-trip signals. That is, an overlaid threshold T_o value different than that employed to collect the data is used. This is possible because the thresholds employed to collect the data is always lower. Although reflectivity is recorded, relative powers from the various trips can easily be computed. Thus, the relative signal powers are calculated (absolute signal power is not needed) as a function of range, and then the calculation of power ratios for weather signals from the various trips is made.

We also used a relatively large *SNR* threshold (i.e., ≥ 15 dB) so that improper estimates of noise are less likely to bias our estimates of true spectrum widths, especially those of small values. To compute the SNR from the reflectivity field requires the radar constant and adjustments for atmospheric attenuation. To simplify the calculation, we assume that all WSR-88D radars have the same performance based upon the WSR-88D specifications (Doviak and Zrnic, 1993, Table 3.1); in short, a reflectivity factor of 0 dBZ at a range of 230 km is assumed to produce a signal equal to noise power. Thus the *SNR*(dB) is calculated from reflectivity factor in dBZ and the formula

$$SNR(dB) = 20\log_{10}\left(\frac{230}{r(km)}\right) + Z(dBZ).$$

Spectrum widths having zero value sometimes appear to be anomalously large in number. Because zero spectrum widths could be due to low *SNR*, narrow widths, and improper measurements of noise power, we have not included zero width values in the statistics to be presented in Section 3.

Editing data for improper setup of the AGC was less quantitative; if positive correlation is detected between large reflectivity values and large spectrum widths in one region, but not in another at about the same range, it is assumed that the AGC is correctly set up. But if there appears to be positive correlation in all regions at about the same range, then the data were not classified.

These editing procedures, although censoring large amounts of data which might also contain correct width estimates, guarantees that the classified data are more accurate and reliable than if the less stringent procedures of the WSR-88D radars were used. Because we have large amounts of data from many radars around the country, and collected for several years, there should be sufficient data to provide meaningful statistics on the relation between spectrum width values and weather classes.

3. Weather classification

We classify the weather into categories which are principally based upon radar observations, and we give examples for each weather class. The various weather types are subjectively identified, and the region encompassing the selected class is enclosed by a hand drawn contour within which the data is processed to gather the statistics of spectrum width. This subjective selection is necessary because any data field could contain more than one class of weather (e.g., strongly convective rain along a squall line and stratiform rain behind it).

3.1 *Clear air*:

Clear air echoes are principally associated with two classes of scatterers; (1) refractive index perturbations, and (2) biological scatterers such as insects and birds. Refractive index perturbations faithfully follow the motions of air parcels, and thus spectrum widths, observed under conditions where only refractive index perturbations principally contribute to the echoes, give true estimates of air parcel motions. Radar measurements of the structure parameter C_n^2 of refractive index, airborne in situ measurements of C_n^2, and numerical models of marine boundary layers, the type that gives rise to the largest perturbations of refractive index, suggest that C_n^2 is rarely larger than about 3×10^{-12} $m^{-2/3}$ (Doviak and Zrnic, 1993; Section 11.6.1). Using the relationships between reflectivity factor Z, reflectivity or cross section per unit volume η, and C_n^2 (Doviak and Zrnic, 1993, Eqs.11.104, and 4.33) this upper limit for C_n^2 corresponds to a reflectivity factor Z less than 0 dBZ for 10 cm wavelength radars. When insects and/or birds are present in large numbers, the spatial distribution of reflectivity may no longer be that associated with point scatterers, but it becomes spatially uniform, and reflectivity factors can be as much as three orders of magnitude larger than that maximum expected for refractive index perturbations.

Clear air weather is declared if the reflectivity factor field is uniform, confined to the first kilometer or two of the atmosphere, and has practically all values less than 10 dBZ. If reported cloud cover data is available, it should be less than 1/10 of the entire sky. Usually visual observations are not available, and some of the clear air cases might have significant cloud cover. Furthermore, because we rarely have visual observations, we have used the 10 dBZ limit in an attempt to eliminate situations where light stratiform rain could satisfy the stipulated conditions for declaring clear air. For example, a 10 dBZ level of reflectivity factor roughly corresponds to a rainfall rate less than 0.15 mm per hour. This is indeed a very light rain and, if present, would not likely be associated with spectrum width values very different from that seen in clear air. Fog has drop sizes too small to be detected by the WSR-88D. On the other hand, the 10 dBZ limit also eliminates those cases of "clear air" in which birds and insects generate values larger than 10 dBZ. If present, birds and insects can cause spectrum widths to be much larger than those values associated with simply air motions (i.e., birds and insects darting about during feeding times can have differential velocities much larger than that associated with shear and turbulence). There is no easy way to separate the contributions that insects and birds make to the spectrum widths, and

we must accept that some of the observed widths under clear air conditions might not be representative of air motions.

Fig. 3a. shows an example of the reflectivity factor field of clear air signals at an elevation angle of 0.5° from KTLX WSR-88D in Oklahoma City, Oklahoma, on May 13, 1998. The fact that Z values are for the most part larger than 0 dBZ suggests that these echoes are from insects/birds. Fig.3b is the associated spectrum width field. In this figure, there are very few areas that have data censored (e.g., the purple colored areas at about 150 km to the west) for which the overlaid threshold of 20 dB is not exceeded. For the most part spectrum widths appear to be less than 7 m s^{-1}. Nevertheless, these are relatively large values, and it is likely that they are associated with biological scatterers that have relatively large differential speeds. In this case the spectrum width values are not representative of air motions.

Other than the small area of large spectrum widths to the northwest at ranges from about 15 to 55 km (i.e., the green yellow patches), the largest spectrum widths with values of 3 m s^{-1} appear to be aligned in direction from southwest to northeast. Lower spectrum widths are noted in orthogonal directions. To determine the cause of this pattern requires further investigation beyond the scope of this study.

Fig. 3c gives an example of the statistics of the spectrum width fields for this clear air case. Because the data is collected in radar or polar coordinates, weather elements close to the radar would have many more points than like elements that are at more distant ranges; thus there would be an unequal weighting of the spectrum width data. Therefore, we have interpolated the data to a Cartesian coordinate system with grid spacings of 250 m, about the best resolution of the radar, so that there are equal number of grid points within a region independent of range. The upper curve in Fig.3c displays the probability distribution (in per cent) of spectrum widths for all elevation angles that have data within the vertical column enclosed by the white hand-drawn contour on Fig.3a, and which meet the specified restrictions (e.g., $SNR \geq 20$ dB; $Z \leq 10$ dBZ). Thus the high reflectivity areas (i.e., the purple to green and yellow coded areas near the radar in Fig. 3a where $Z > 10$ dBZ), which are likely contaminated with effects of ground clutter, are not included in the statistical summaries for clear air.

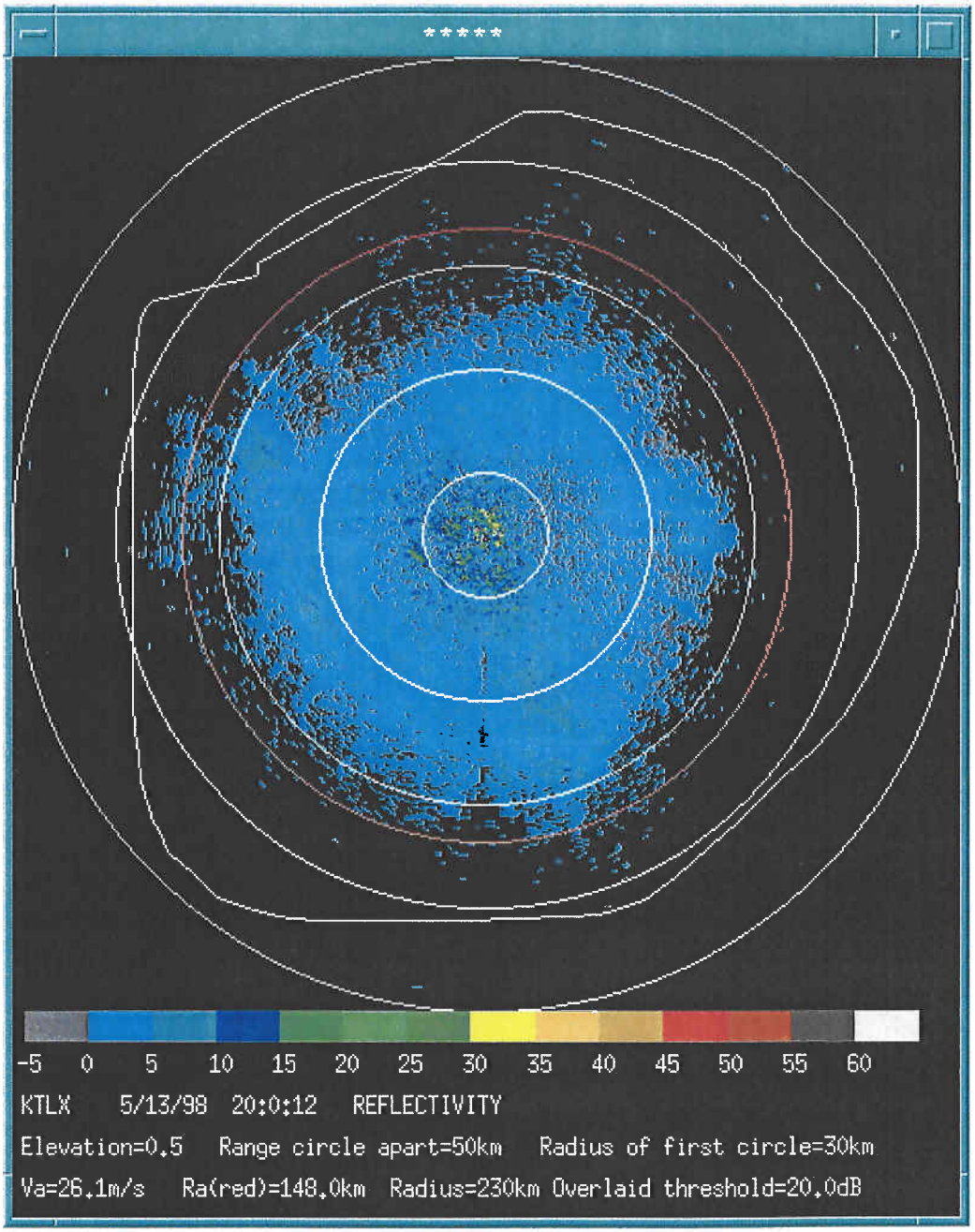

Fig. 3a The clear air reflectivity factor from the KTLX WSR-88D radar in Oklahoma City, OK on 13 May 1998 at 20:00 UT. Elevation angle is 0.5°. The white contour outlines the volume within which the probability distribution (Fig. 3c upper curve) of widths is presented.

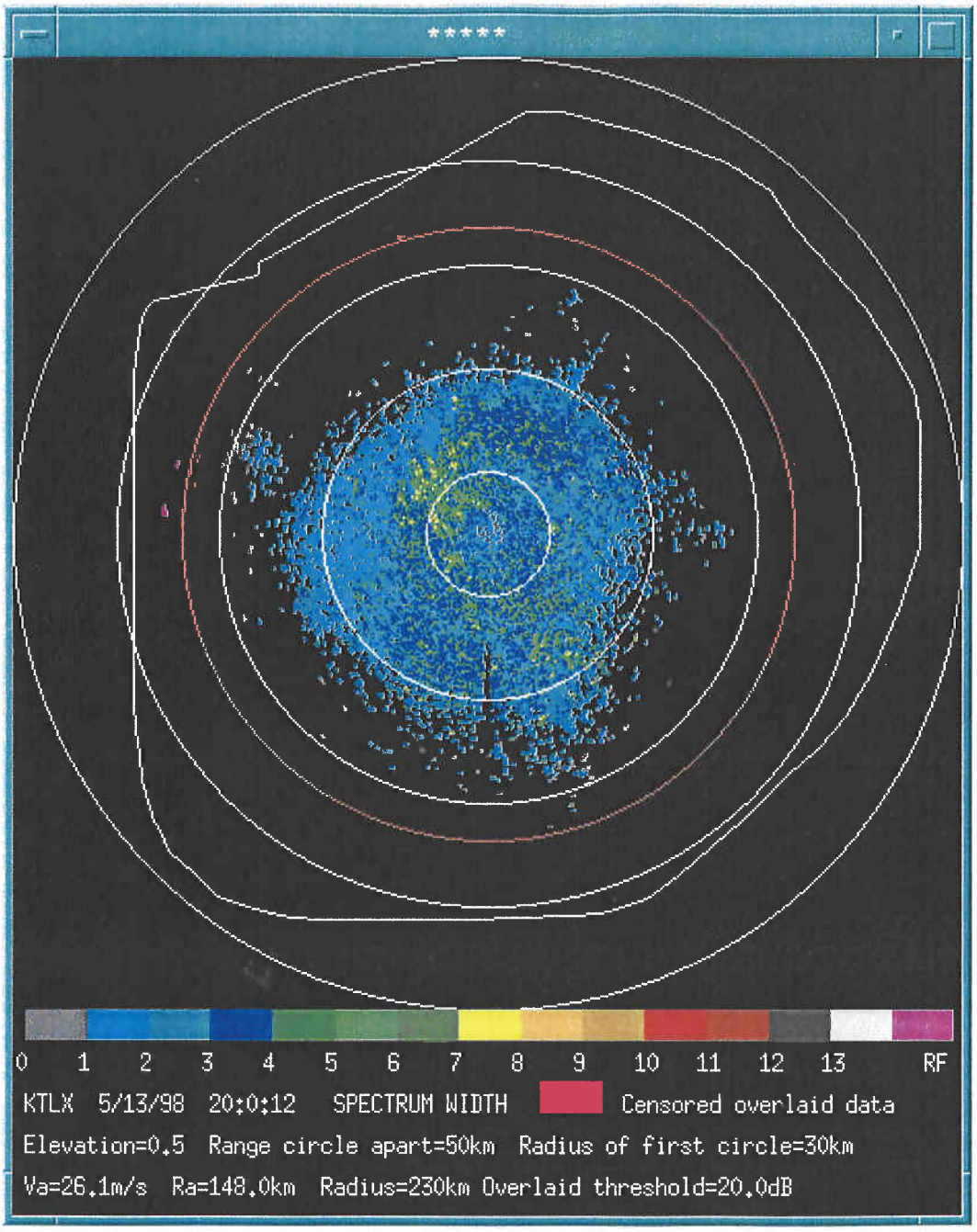

Fig. 3b The spectrum width field corresponding to Fig. 3a.

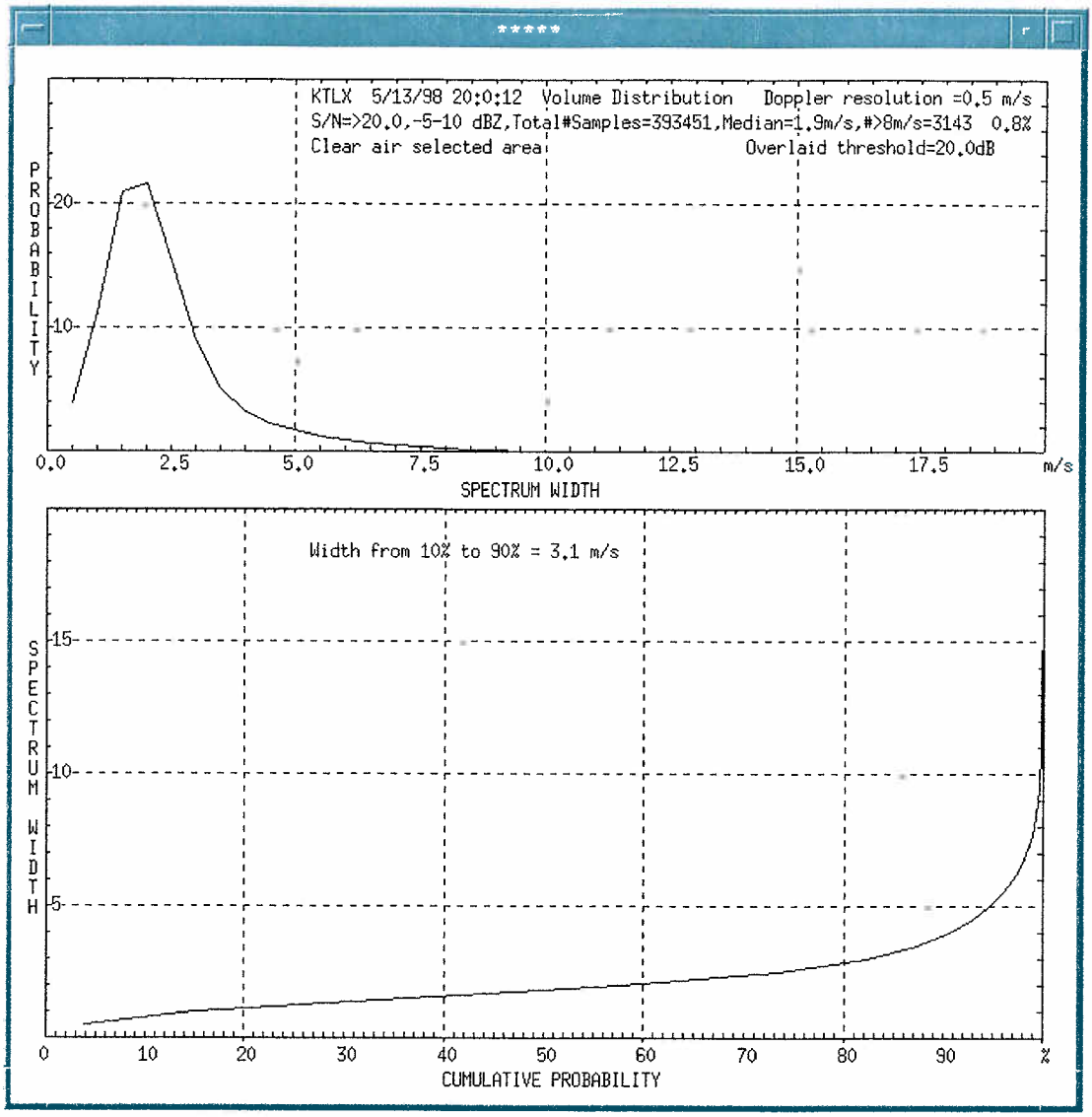

Fig.3c. The probability (upper curve) and the cumulative probability for spectrum widths in clear air (see Fig. 3a for data collection area). The data are from the entire volume enclosed by the hand-drawn white contour in Fig. 3b (data void regions are colored black).

The spectrum width data are provided with a 0.5 m s^{-1} resolution, and these data are therefore accumulated into 0.5 m s^{-1} intervals for presentation in Fig. 3c to provide a probability curve (the upper curve). The probability is the per cent of total data that lie within a selected interval; zero values are not counted. The lower plot is the cumulative distribution, also for the entire volume (i.e., all elevation angles at which there is data within the drawn contour). We derive the median value of spectrum width from the cumulative distribution. The relatively uniform slope of the cumulative curve for widths lying between the 20 and 80 percentile points is a characteristic of most of the spectrum width data analyzed, and is due to the Gaussian shape of the probability curve about the median value. Also indicated on this figure is the total number of grid points, and the per cent of data for which the spectrum width exceeds 8 m s^{-1}.

An 8 m s^{-1} value is chosen because simulations of the performance of the SZ phase code algorithms to separate overlaid signals (to estimate Doppler velocities associated with the weaker signal) suggest that separation is unlikely for spectra with widths larger than 8 m s^{-1} (Sachidananda, 1998). This limit is dependent, however, on the ratio of overlaid signal powers and the width of both, if there are two, spectra. For example if the width of the weaker signal is about 4 m s^{-1}, and it has power 10 dB below the stronger signal, separation of signals is possible if the spectrum width of the stronger signal is less than about 7 m s^{-1} (Sachidananda, 1998, Fig. 5.6).

3.2 *Stratiform rain*:

Stratiform rain is assumed if the reflectivity field is fairly uniform over large areas, and has values less than about 40 dBZ. Using the representative and useful, although not always correct, relation (Doviak and Zrnic, 1993, Eq.(8.22a))

$$Z_w \text{ (dBZ)} = 23 + 16 \log_{10}[R(\text{mm h}^{-1})] ,$$

between the stratiform rain rate R and the reflectivity factor Z_w of water spheres, where Z_w is obtained from application of the radar equation (i.e., Eq.4.35 in Doviak and Zrnic, 1993), 40 dBZ corresponds to a rainfall rate of 11.5 mm h^{-1}. Stratiform rain could be associated with warm fronts in which warm moist air overrides a pool of heavier cold air, or it could be associated with the stratiform rain area behind squall lines, or that which evolves from convective precipitation systems.

Fig. 1a gives the reflectivity factor field of an example of a stratiform rain case from KDMX WSR-88D radar in Des Moines, Iowa, on May 27, 1995. As presented earlier, Fig. 1d is the spectrum width field at 0.5° elevation angle, using the overlaid threshold T_o = 20 dB and is the threshold value used for all the reported statistical results. Notice the area of large spectrum widths to the southwest of the radar at ranges from about 100 km to 150 km that have survived the more stringent data censoring thresholds and are likely true values. These regions propagated northeastward, and because they were found an hour later in regions of relatively high reflectivity (i.e., > 30 dBZ), and because the reflectivity in the second trip region that could have overlaid

this first trip region was less than -6 dBZ, further support is obtained that these high spectrum width regions are valid. Nevertheless they are large, and the meteorological reason for these large values in stratiform rain requires further investigation.

Fig. 4 gives the statistics of the spectrum width field in the volume of data in the vertical column out to a range of 230 km, and that have associated reflectivity values between 20 and 40 dBZ. Regions with reflectivity factors less than about 20 dBZ could contain echoes from insects and birds. Here and for some of the other classifications of spectrum width in rain showers, a 20 dB threshold on the lowest reflectivity factor is used to eliminate, from the statistical analysis, those spectrum widths that are likely to be associated with echoes from clear air biological scatterers. Of course drawing a contour around the phenomena of interest also restricts our analysis to those selected weather classes.

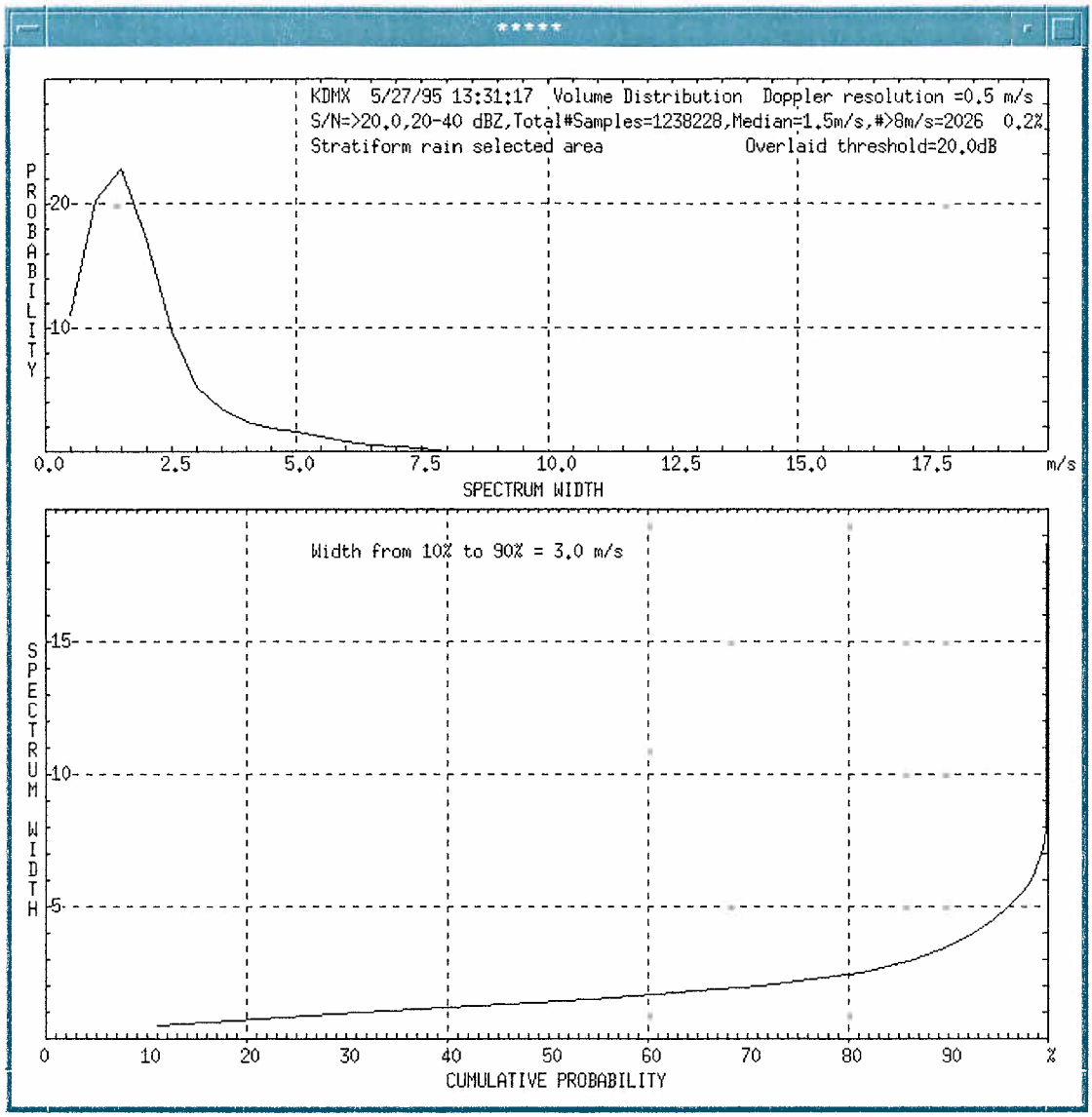

Fig. 4. The probability and cumulative probability of spectrum widths for stratiform rain (See Fig. 1 for the reflectivity and spectrum width fields at 0.5° elevation angle). The data are from the entire volume of stratiform rain out to a range of 230 km.

3.3 *Widespread weak showers*:

Widespread weak showers are, for the most part, numerous isolated convective cells having peak reflectivity factors less than 45 dBZ, but at least some of the cells must have a peak reflectivity value more than 35 dBZ. Each cell typically has diameters less than about 10 km..

The area of showers enclosed by the white contour in the reflectivity factor field of Fig.5a gives an example of widespread weak showers recorded by KTBW WSR-88D radar in Tampa, Florida, on March 3, 1998. The white contour was drawn to enclose only those convective cells which had a core reflectivity value less than 45 dBZ. Fig.5b is the corresponding spectrum width field in the vertical column enclosed by the white contour. It is noted that the few excluded cells in the widespread shower region that had Z values larger than 45 dBZ have spectrum widths that do not differ from those within the contour; however this is not so for those larger reflectivity cells along the squall line to the southeast of the radar. This demonstrates the necessity to subjectively determine the areas which need to be analyzed. Fig.5c gives an example of the statistics of the spectrum width in the region of widespread weak showers.

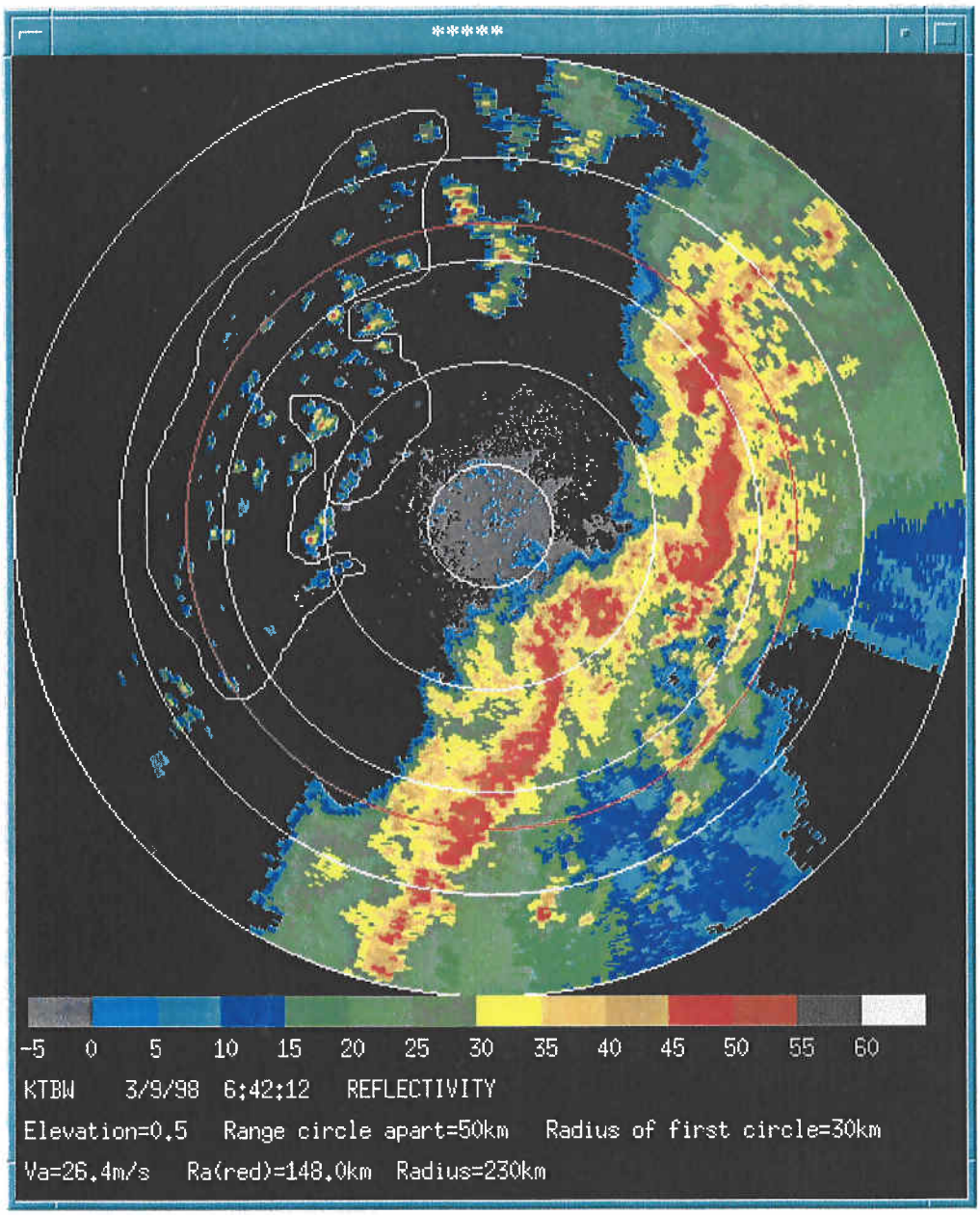

Fig. 5a The reflectivity field for wide spread showers (i.e., the convective cells enclosed by the white contour). The KTBW radar is located in Tampa Florida and data were collected on 9 March 1998 at 06:42 UT.

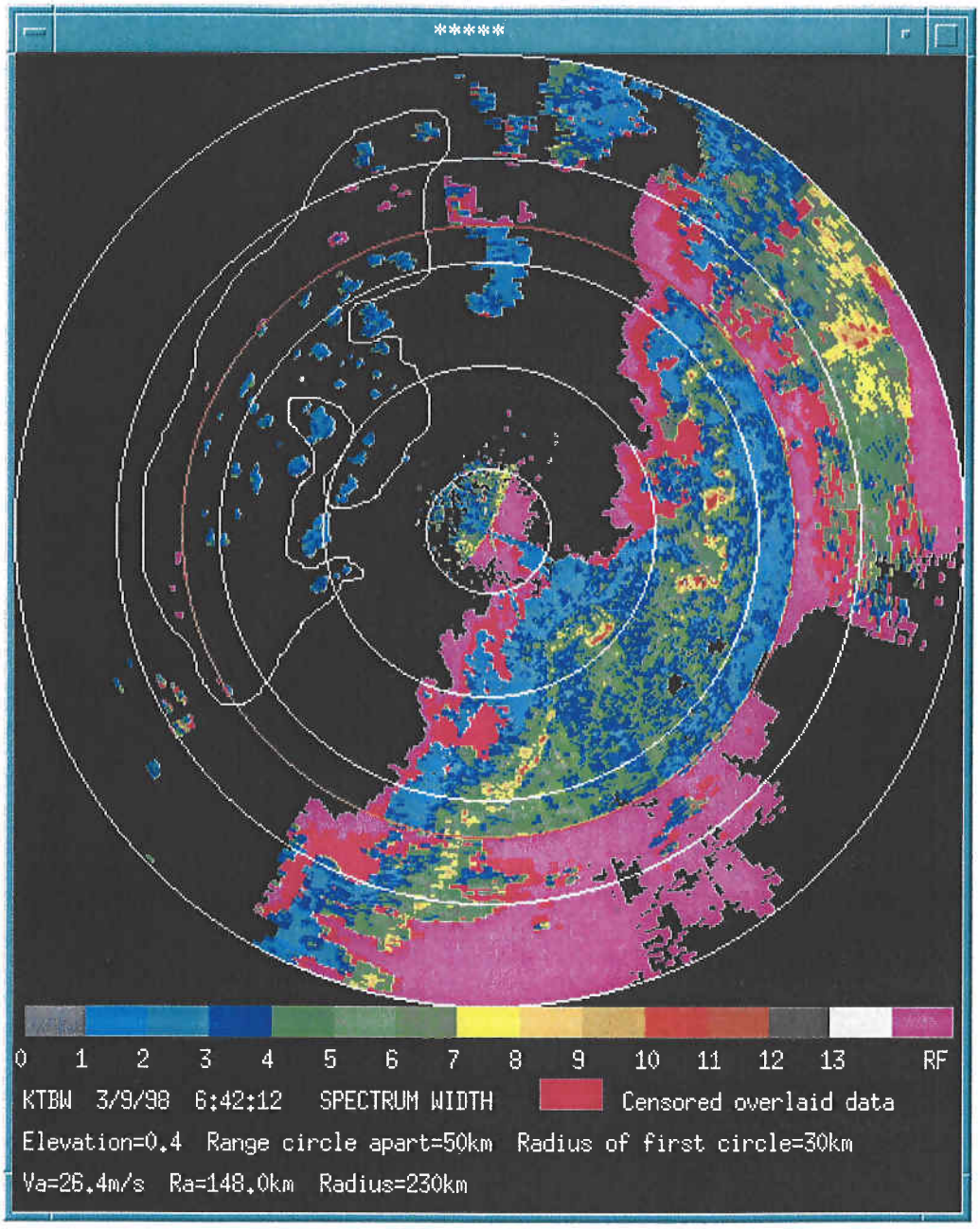

Fig. 5b The spectrum width field corresponding to Fig. 5a.

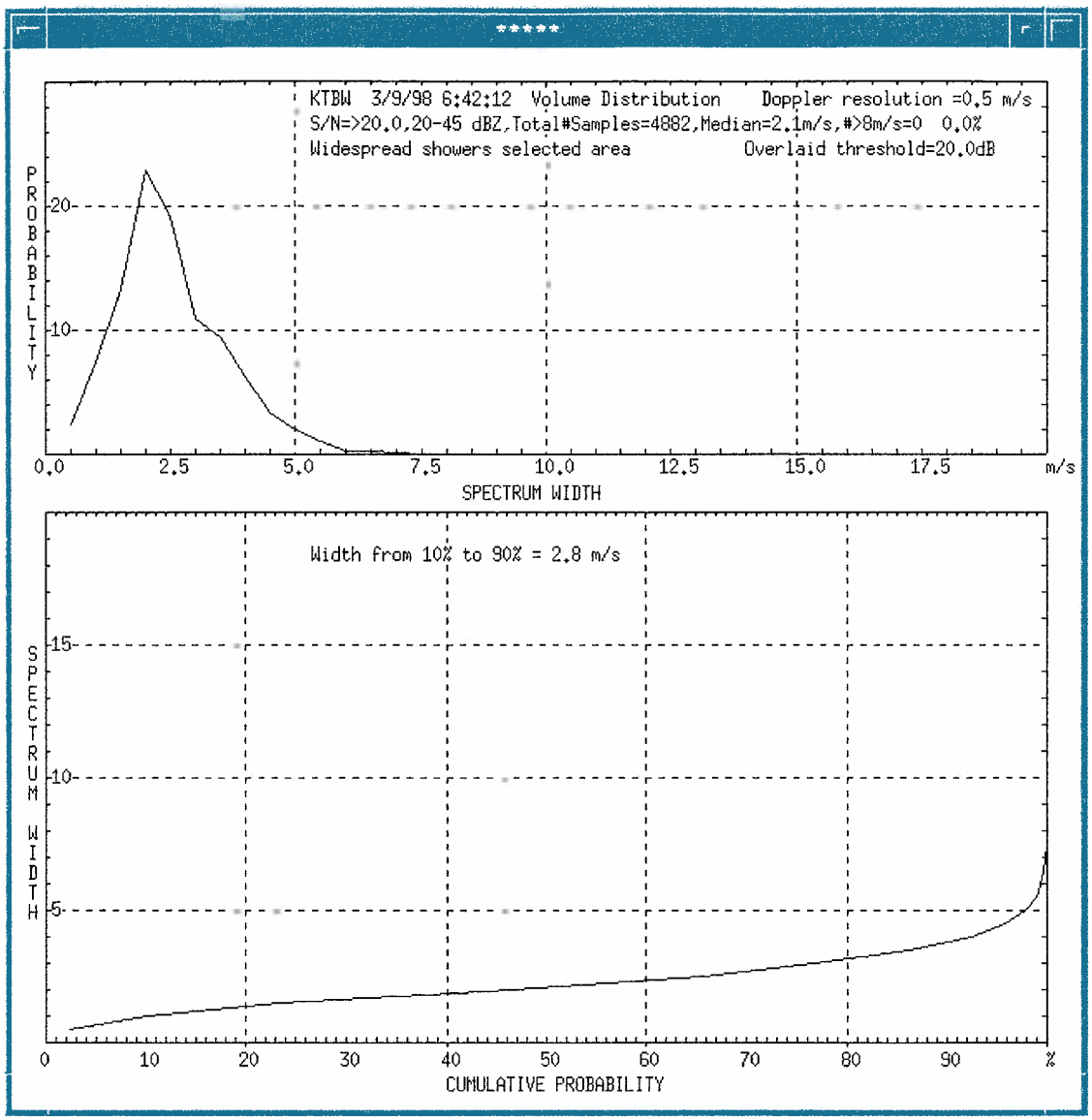

Fig. 5c. The statistical properties of the spectrum width field for widespread showers (i.e., the showers enclosed by the white contour in Fig. 5a).

3.4 *Isolated severe storm*:

Isolated severe storms are convective cells far from other severe storms which could significantly disturb the environment flow into the isolated storm. Storms are considered severe if they have large areas in which the peak reflectivity factor is higher than 45 dBZ. These cells usually contain damaging winds, hail, and tornadoes.

An example of the reflectivity factor field of a system of severe storms is presented in Fig.6a, and the isolated severe storm is enclosed with the hand drawn white contour. The data was collected by the KCRI WSR-88D radar south of Oklahoma City on May 3, 1999 at 23:57 UT. At this time the storm was producing a tornado which devastated Moore, Oklahoma. The white contour encompassing this storm serves to isolate the spectrum width statistics of the isolated severe storm from those width values associated with the multi-cell severe storms to the far northwest.

Figs.6b and 6c are the corresponding Doppler velocity and spectrum width fields. Because a relatively large unambiguous range (i.e., 177 km) was selected, and because the storms are not wide spread, there is no evidence of first trip data being censored because of overlaid echoes. Noteworthy from Fig.6c is that spectrum widths associated with the multi-cell storms to the northwest, and even those spectrum widths of the clear air to the south and southeast, are significantly larger than those within the isolated severe storm. That spectrum width values are larger for the multi-cell storms is consistent with the fact that the velocities (Fig. 6b) in these storms show much larger spatial variability than the velocity field in the isolated tornadic storm. Thus, it appears that the flow within the isolated tornadic storm is less turbulent than the flow within the multi-cell storms, some of which are also tornadic.

Figs. 6d and 6e present the statistical data for this isolated storm, and show the statistics of spectrum width from regions where reflectivity factor ranges from 40 to 70 dBZ (i.e., the core of the storm) and those regions where reflectivity factor ranges from 20 to 40 dBZ (i.e., the light precipitation regions surrounding the strongly convective part). Noteworthy is that the spectrum width distributions are nearly identical suggesting that turbulence inside the storm core is the same as that in the environment outside the storm. This is consistent with an apparently laminar flow in and around this tornadic storm.

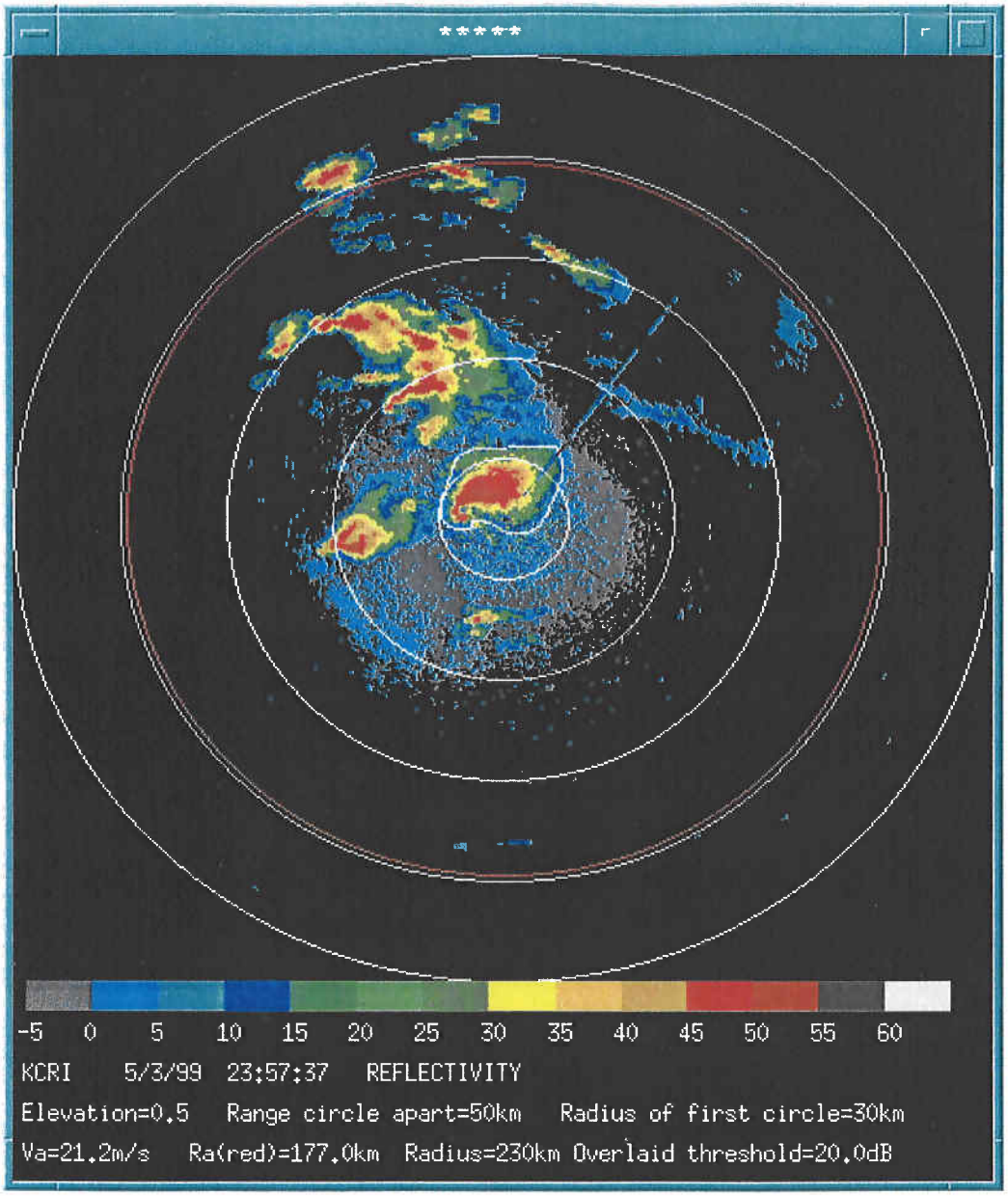

Fig. 6a The reflectivity factor field of severe tornadic storms in Central Oklahoma. The storm encircled with the drawn white contour is the isolated tornadic storm that devastated Moore Oklahoma and is the region where statistics of spectrum width are derived.

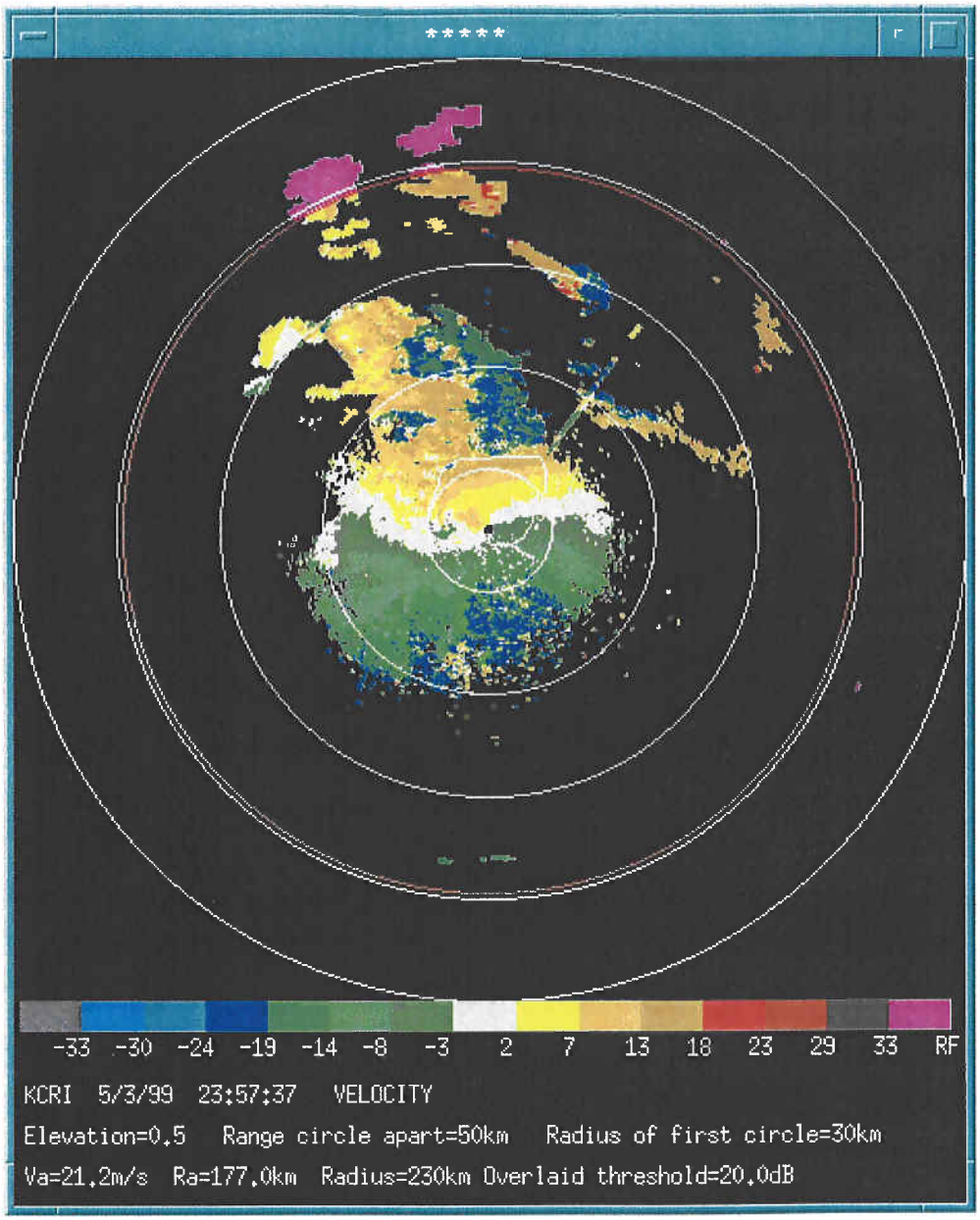

Fig. 6b The Doppler velocity field corresponding to the data in Fig. 6a. Note the relatively smooth Doppler velocity field in the Moore OK storm, suggestive of laminar flow, whereas the severe storms to the NW exhibit higher spatial variance.

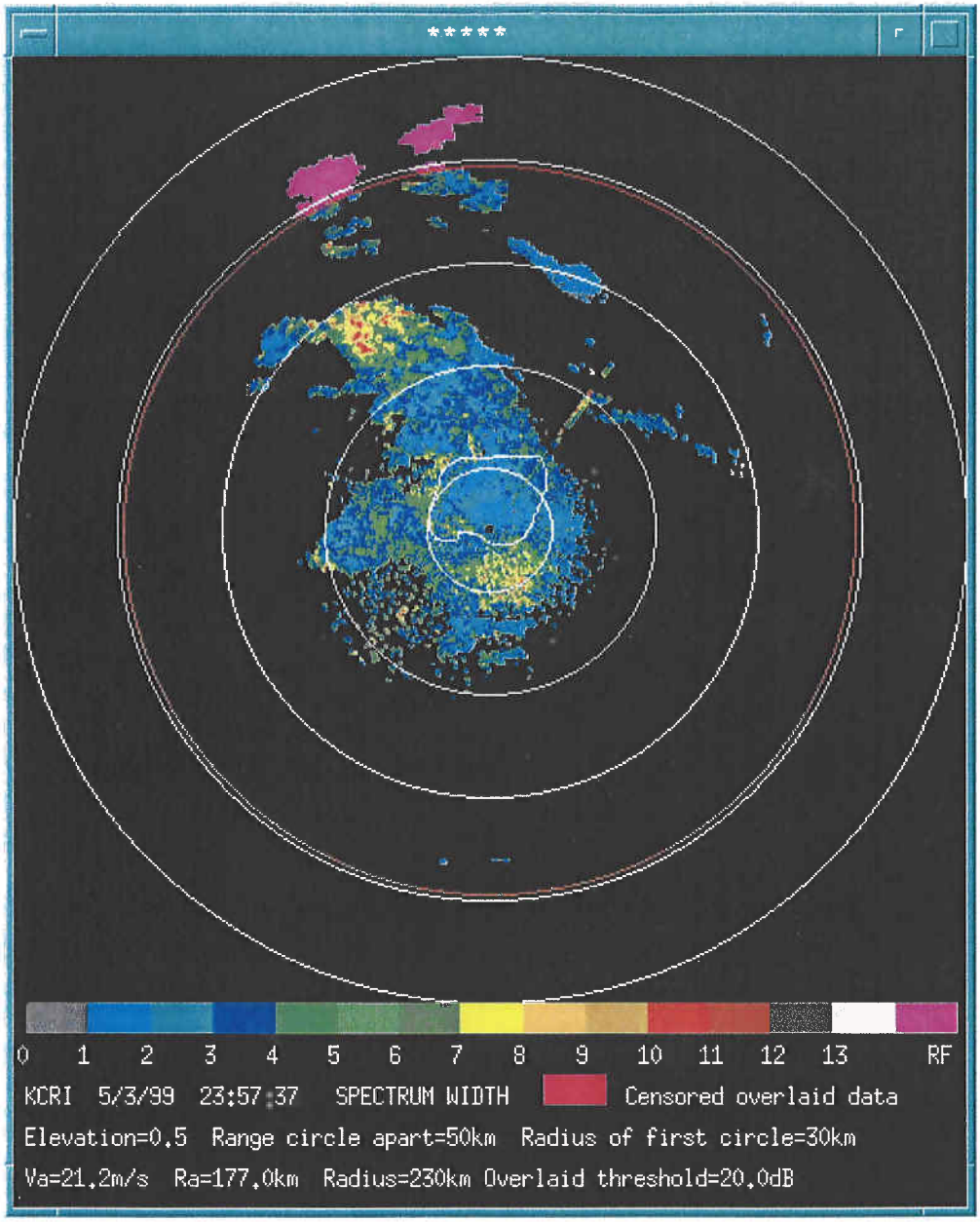

Fig. 6c The spectrum width field associated with Fig. 6a. Spectrum width values of the isolated tornadic storm are enclosed by the white contour and are those analyzed. Compare the spectrum widths in this isolated storm with those in the cluster of severe storms to the NW.

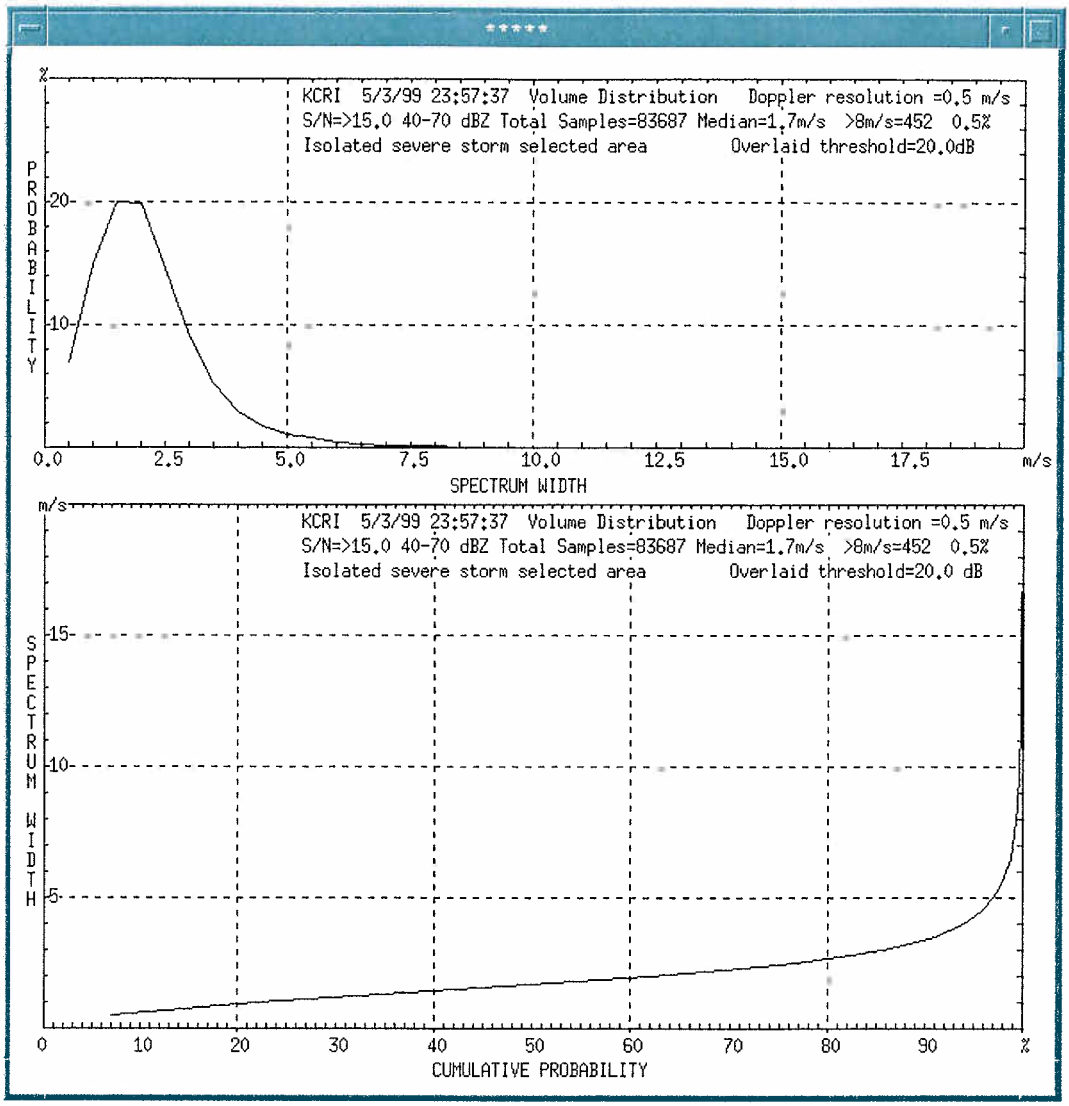

Fig.6d The statistical properties of the spectrum width field of the Moore OK storm in regions where the reflectivity factor lies between 40 and 70 dBZ.

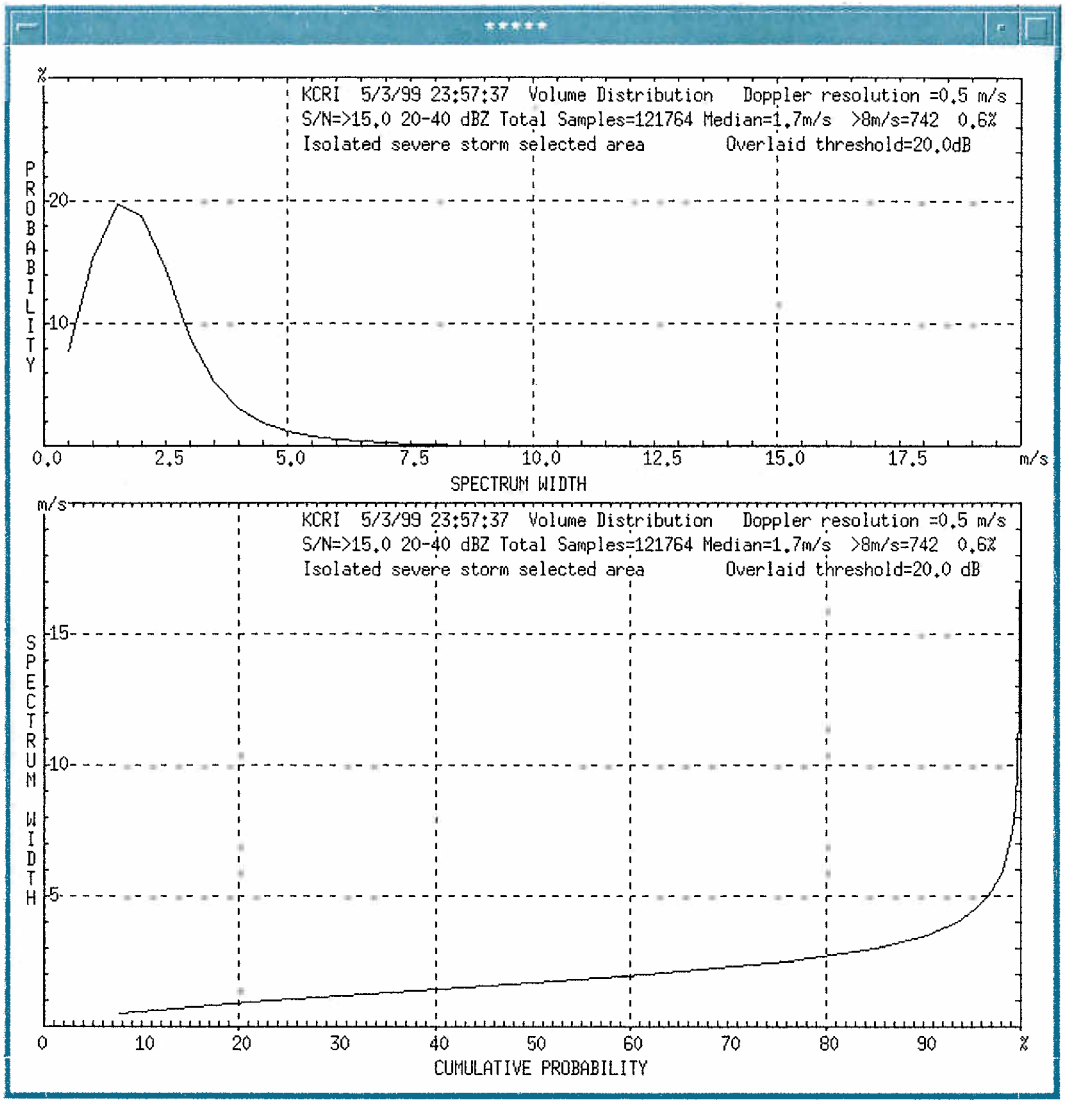

Fig. 6e The statistics of spectrum width in regions of an isolated severe storm where reflectivity factor lies between 20 and 40 dBZ.

3.5 *Multi-cell severe storms*:

Multi-cell storms are clusters of convective cells that are closely spaced (less than about 20 km), and have reflectivity factors higher than 45 dBZ.

An example of the reflectivity factor field of multi-cell severe storms is the area outlined by the white contour sketched onto Fig. 7a. The corresponding velocity and spectrum width fields, in the vertical column outlined by the white contour, are presented in Figs. 6b, and 6c. The statistics of spectrum width for the reflectivity categories 20 to 40 dBZ, and 40 to 70 dBZ are presented in Figs. 7b and 7c. Note that these multi-cell storms have, on average, larger spectrum widths than the isolated severe storm to the south which was occurring at the same time. Also note that the spectrum width fields in the weaker reflectivity regions surrounding the storm cores have significantly smaller widths than the corresponding core regions; the median value is 2.6 m s^{-1} whereas the storm core regions have a median value of 3.8 m s^{-1}. The median value of 3.8 m s^{-1} is in close agreement with that found by Doviak and Zrnic (1993, Fig. 10.11) for three tornadic storms, but their data was for all reflectivity regions having a SNR > 15 dB. The median value for all the data having spectrum width values from 20 to 70 dBZ computes to be 2.9 m s^{-1} and this value is listed in Table 2 to be presented later. Thus, the medium value for the cluster of severe storm cells and their immediate environment enclosed by the white contour drawn on Fig.7a, is somewhat lower than that found by Doviak and Zrnic. Further investigation is need to determine whether this difference is significant and related to the structure of the storms and the areas analyzed.

6.7% of the widths in the core region have values exceeding 8 m s^{-1} , whereas this percentage drops to 1.8% for the region surrounding the core. The large values of spectrum width found in multi-cell severe storms (i.e., severe storm cells in a cluster), suggest that severe storm cells in the near vicinity of one another are more turbulent. This increase in turbulence might be due to the fact the nearby storm cells might be enhancing the turbulence in the environment surrounding the cores; note that in the case of the isolated tornadic storm, the spectrum width values outside the storm core are almost identical to that inside the core, both of which are significantly less than that found in the regions of the multi-cell storms.

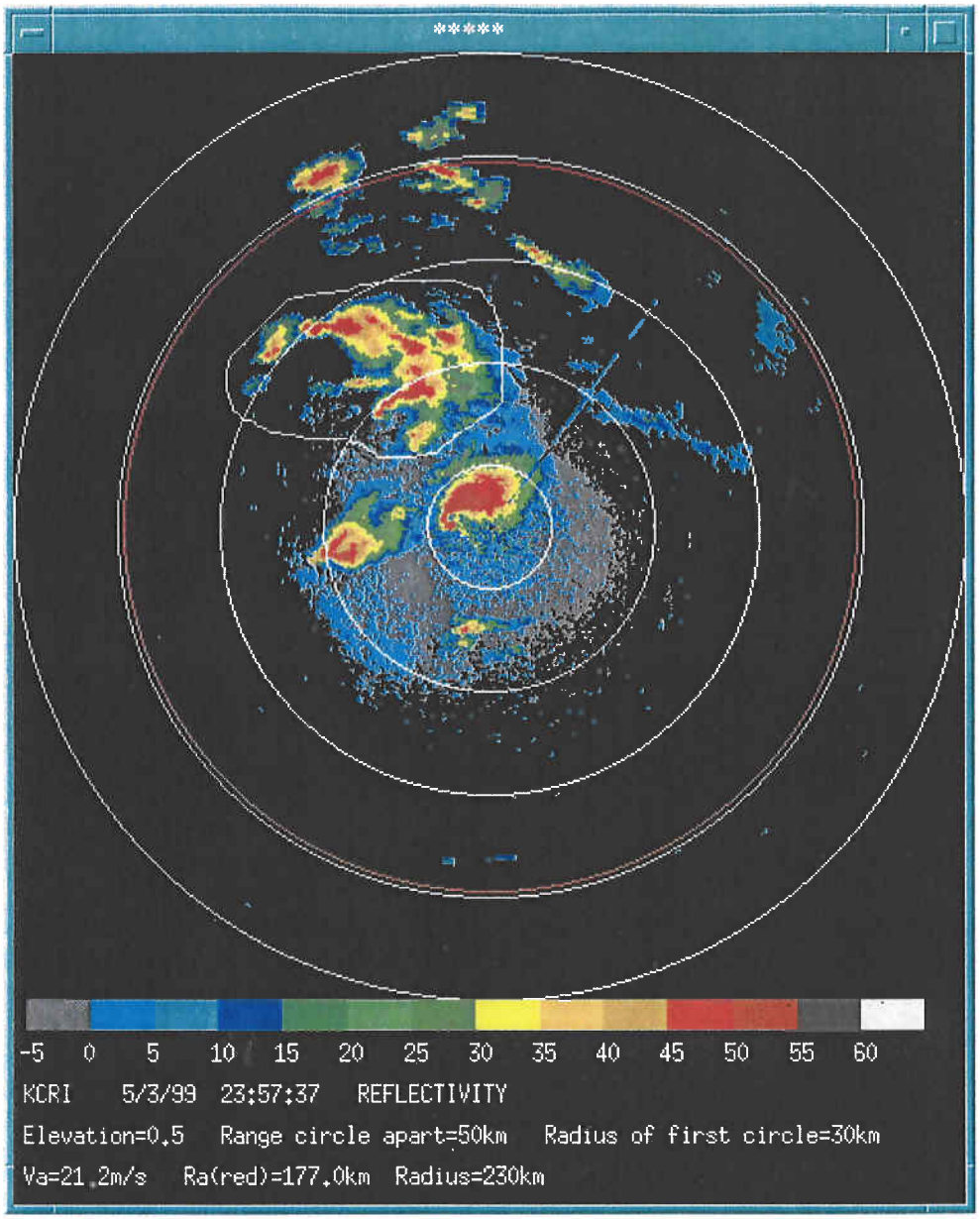

Fig. 7a The reflectivity field of multi-cell severe storms (the storms encompassed by the white contour) used in the analysis.

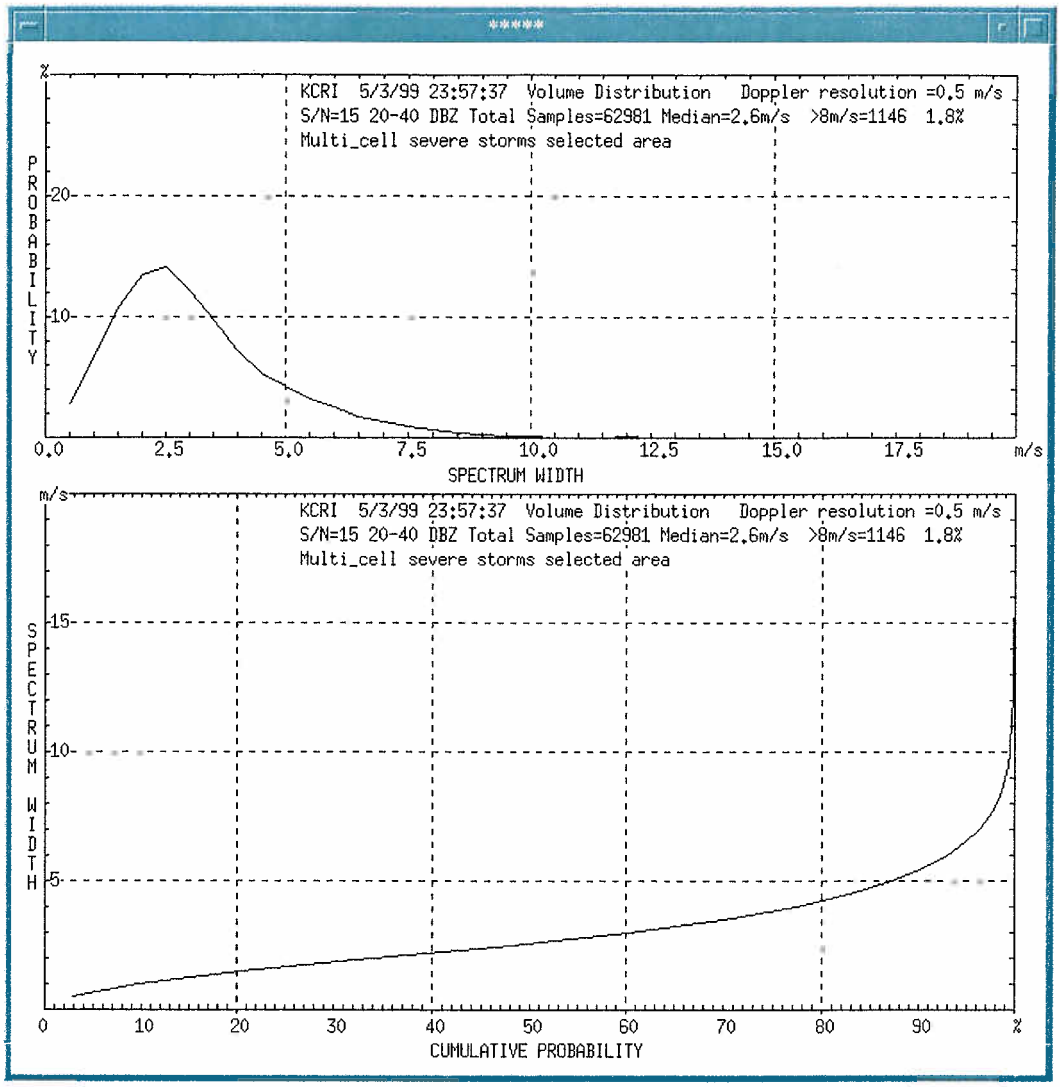

Fig. 7b The statistics of spectrum width for the storms enclosed by the white contour drawn on Fig. 7a, and for regions where the reflectivity factor lies between 20 and 40 dBZ.

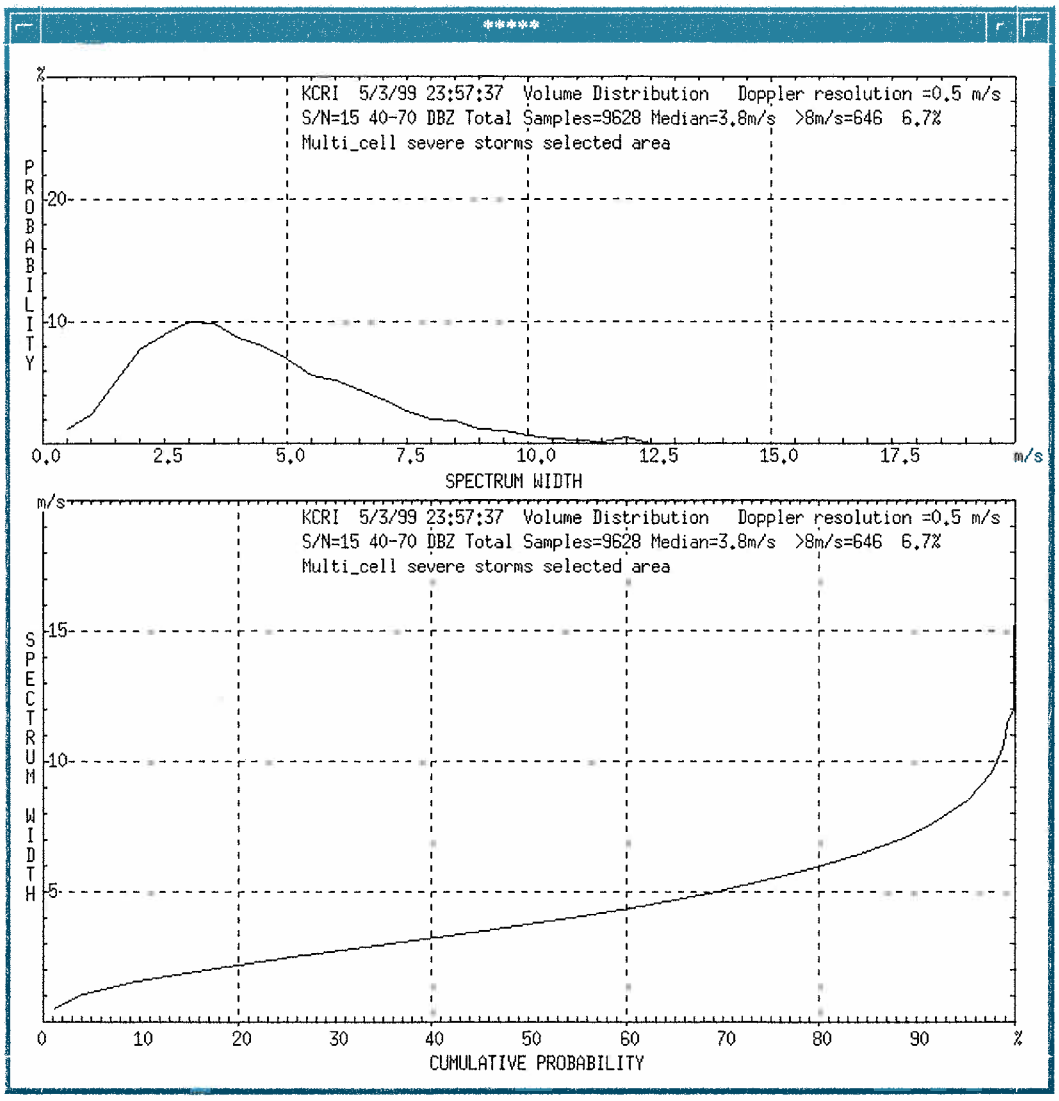

Fig. 7c The statistics of spectrum width for regions of multi-cell severe storms where the reflectivity factor lies between 40 and 70 dBZ.

3.6 *Squall lines*:

Precipitation associated with squall lines appear in bands of strong convection as well as in a trailing stratiform region, but we only examine the statistics of spectrum width in regions of strong convection enclosed by the hand drawn contours, and where the reflectivity factor values exceed 20 dBZ. That is, we do not include the spectrum widths from the trailing stratiform region.

Fig.8a presents the reflectivity factor field of a squall line. This data was recorded by KTBW WSR-88D radar in Tampa, Florida, on March 9, 1998. The large reflectivity band of the squall line is embedded in a wide area of stratiform precipitation. This type of weather is defined as an "embedded areal" squall line (Bluestein, 1993, Fig. 3.72); in a table presented later, these squall lines are simply called "embedded" to differentiate them from "early broken" lines (i.e., the lineal juxtaposition of separated storms in the early stages of squall line development in which there is no stratiform region, and mature broken which are similar to the early broken but the line is formed of mature and/or decaying storms late in the squall lines life which typically lasts 6 to 12 hours (Bluestein, 1993, p. 533).

Fig. 8b shows the Doppler velocity field associated the embedded areal squall line whose reflectivity field is given in Fig. 8a. Note the large shear of the velocity field along the leading edge of the rain band; this shear region defines the leading edge of the thunderstorm outflow where there is usually a sudden shift in mean wind speed and wind direction, and wind is much more gusty (i.e., turbulent). Usually there is a drop in air temperature in the outflow air. The advancing front of cold turbulent air is often referred to as the gust front.

Also note the large variability of the velocity field in the stratiform region behind the southeasterly moving squall line. This suggest that turbulence is significant in the stratiform region as well. Fig. 8c presents the spectrum width field associated with Figs. 8a and b. Note the large spectrum widths along the gust front that continues to the north where Doppler velocity gradients are small because of geometry, and thus the gust front is not visible in the velocity display in those regions. But it is readily discerned in the spectrum width field.

In Fig.8c, the largest spectrum widths in the region enclosed by the white curve lie on the leading edge of the precipitation (i.e., the leading edge of the high reflectivity band), and coincides with the large wind shear line seen in Doppler velocity field. So these large values of spectrum width are associated with wind shear produced by the outflow. But how much of the turbulence lies in scales larger than the beamwidth requires further examination along the lines followed by Istok and Doviak (1986).

Noteworthy, there is another large spectrum width region between 180 km and 230 km from west to northwest. This region of large spectrum widths might be evidence of violent turbulence in stratiform rain. According to Lee (1977), there is a strong connection between the spectrum width and aircraft penetration measurements of turbulence. His data show that if

aircraft-derived gust velocities exceeded 6 m s^{-1}, corresponding to moderate to severe turbulence, the spectrum width exceeded 5 m s^{-1} in every case for aircraft within 1 km of the radar resolution volume. It is possible that aircraft can be vectored into this potentially hazardous region because it satisfies criterion for safety of flight around storms. That is, based on turbulence measurements by aircraft penetrating thunderstorms, and reflectivity measurements with radars, the Federal Aviation Administration (FAA, 1978) has recommended that aircraft remain more than 20 km from the edge of the storm, usually defined as the 20 dBZ contour of severe thunderstorms. Unfortunately, these criteria are often ignored, sometimes with devastating consequence. The large stratiform region, far from the strongly convective squall line, might be where aircraft pilots, waiting for the squall line to pass over the airport, might be lured into landing in this region of stratiform rain because it is far from the squall line, but yet this region could harbor moderate to severe turbulence. To verify whether the regions of large spectrum width far removed from the squall line are indeed a hazard to safe flight, requires in situ measurements. Furthermore, we should determine the shear contribution to spectrum width, as done by Istok and Doviak (1986), in order to remove the large scale shear contributions that do not produce turbulence hazardous to safe flight.

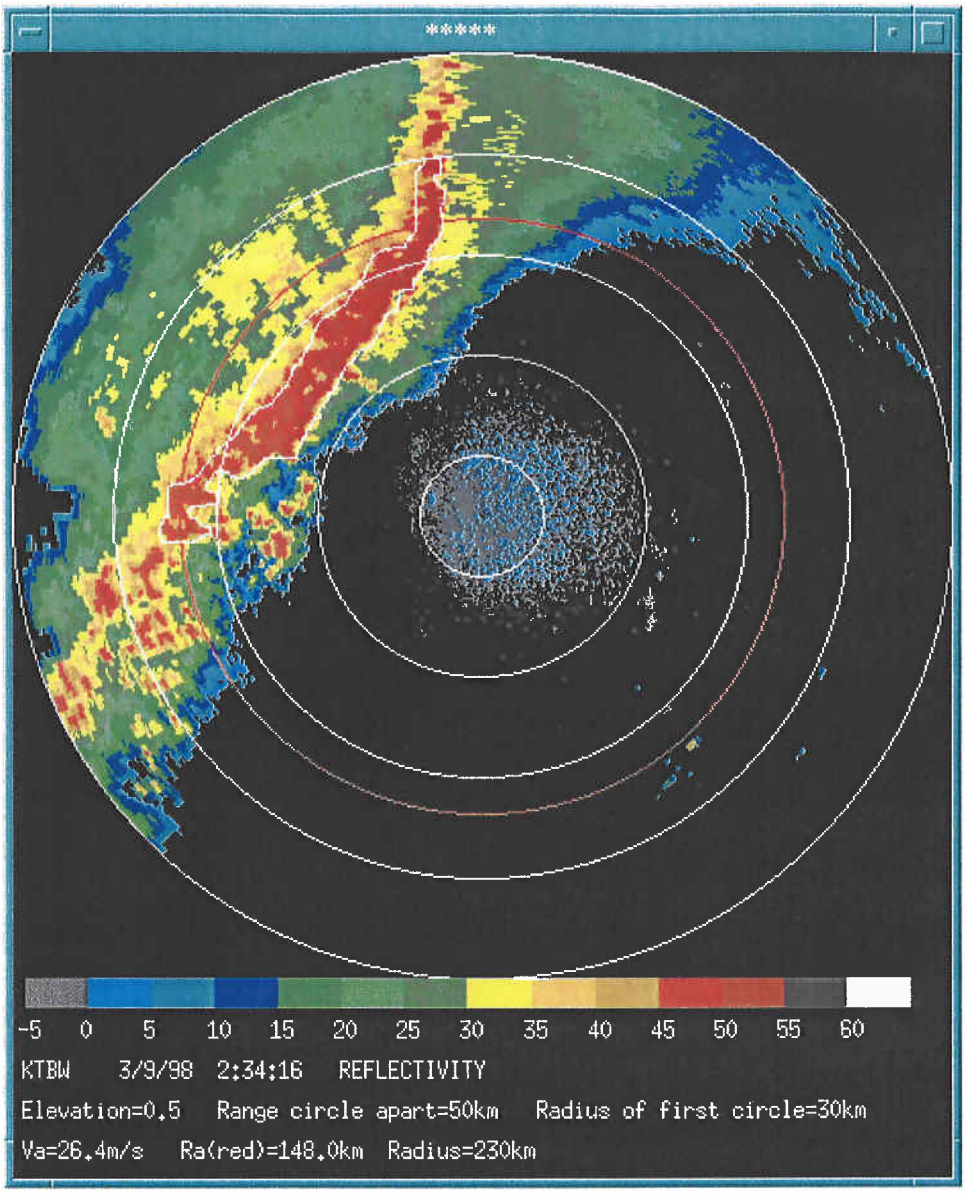

Fig. 8a The reflectivity field of a squall line observed by the KTBW WSR-88D in Florida. The area enclosed by the drawn white curve is that region where analysis of spectrum width data was made.

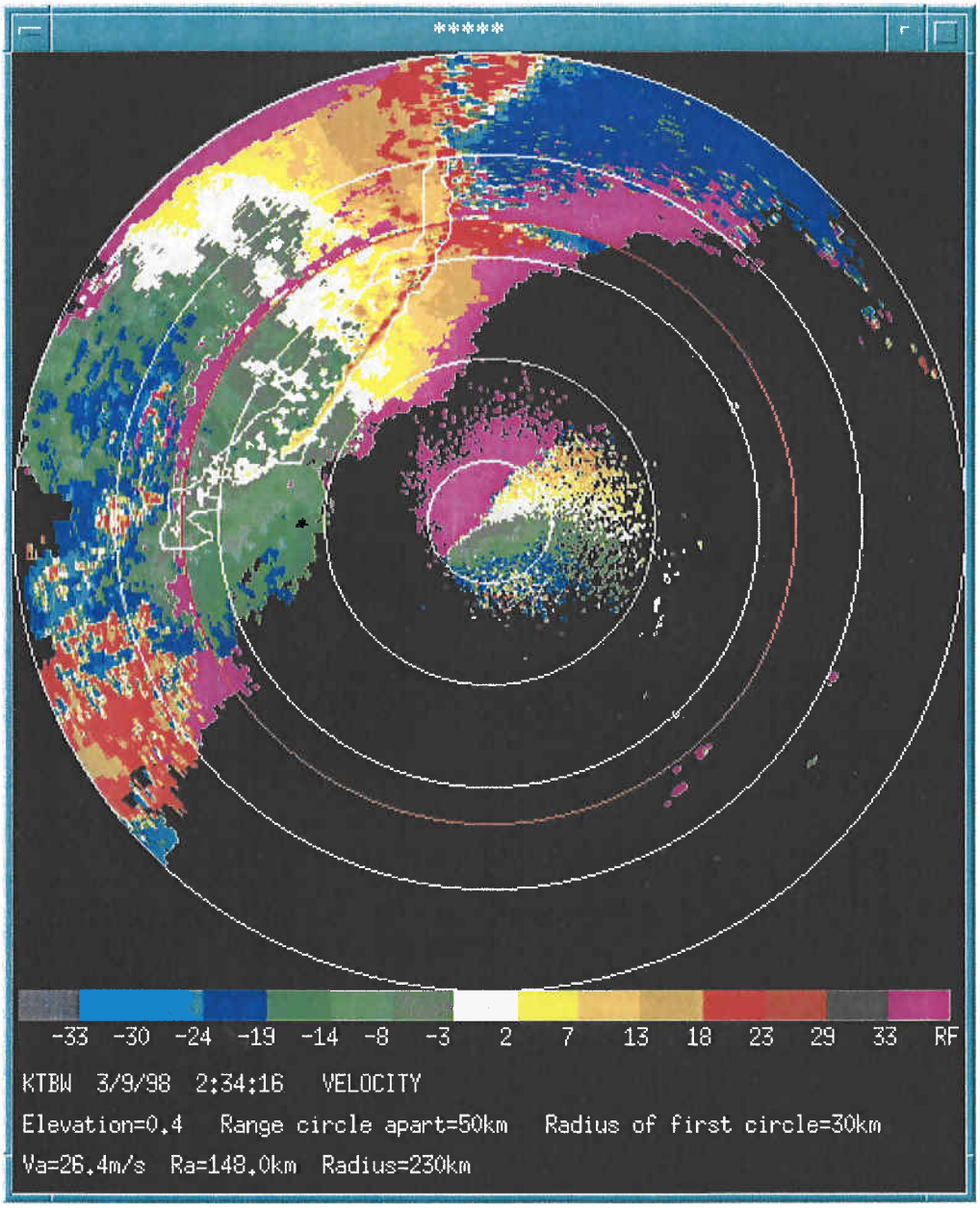

Fig. 8b The Doppler velocity field associated with Fig. 8a. Note the large variability of the velocity field in the stratiform region behind the southeasterly moving squall line.

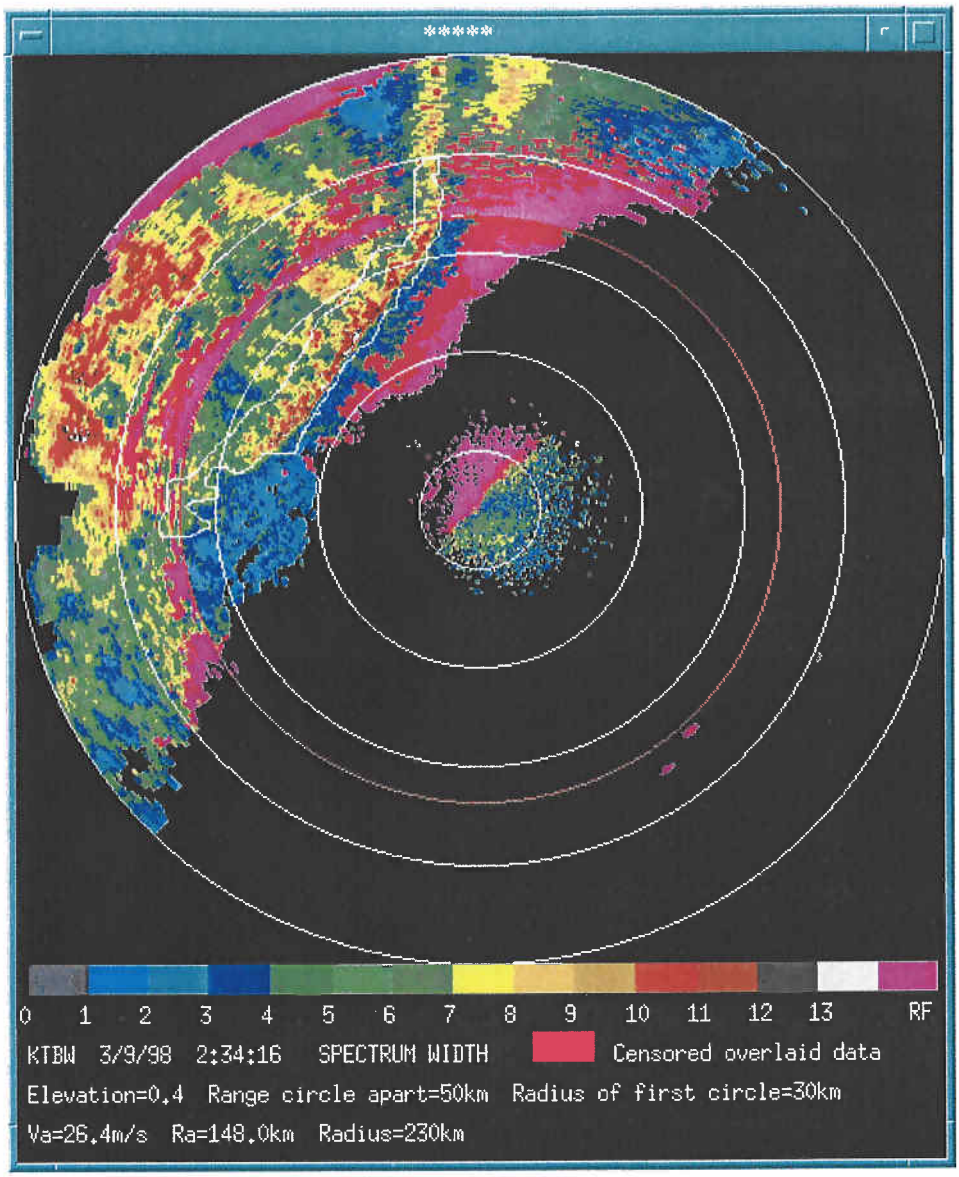

Fig. 8c The spectrum width field of the squall line. Note the large spectrum widths in the stratiform region of the squall line; these appear to be correlated with large spatial variability of the Doppler velocity.

Fig. 8d presents the spectrum width field associated with Fig. 8c, but at an elevation angle of 3.3°. Note the ring of enhanced spectrum width values at the relatively constant range of 100 km. This feature suggests a layer of shear at an altitude of about 6.3 km, and it might also be the same shear layer responsible for the large spectrum widths seen at long ranges in Fig. 8c. The spectrum width values along the squall line's rain band continue to be large, but take on the appearance of separated convective elements.

Fig. 8e presents the statistics of spectrum width for the entire volume of the squall line whose cross section at 0.5° elevation angle is outlined by the white contour in Fig.8a, and for which the reflectivity factor values fall in between 20 dBZ and 70dBZ. Note the large percentage (i.e., 15.5 %) of widths exceeding 8 m s^{-1}. This and the large median value of spectrum width along the convective portion of the squall line, suggests that this class of weather is the most turbulent and hazardous to safety of flight.

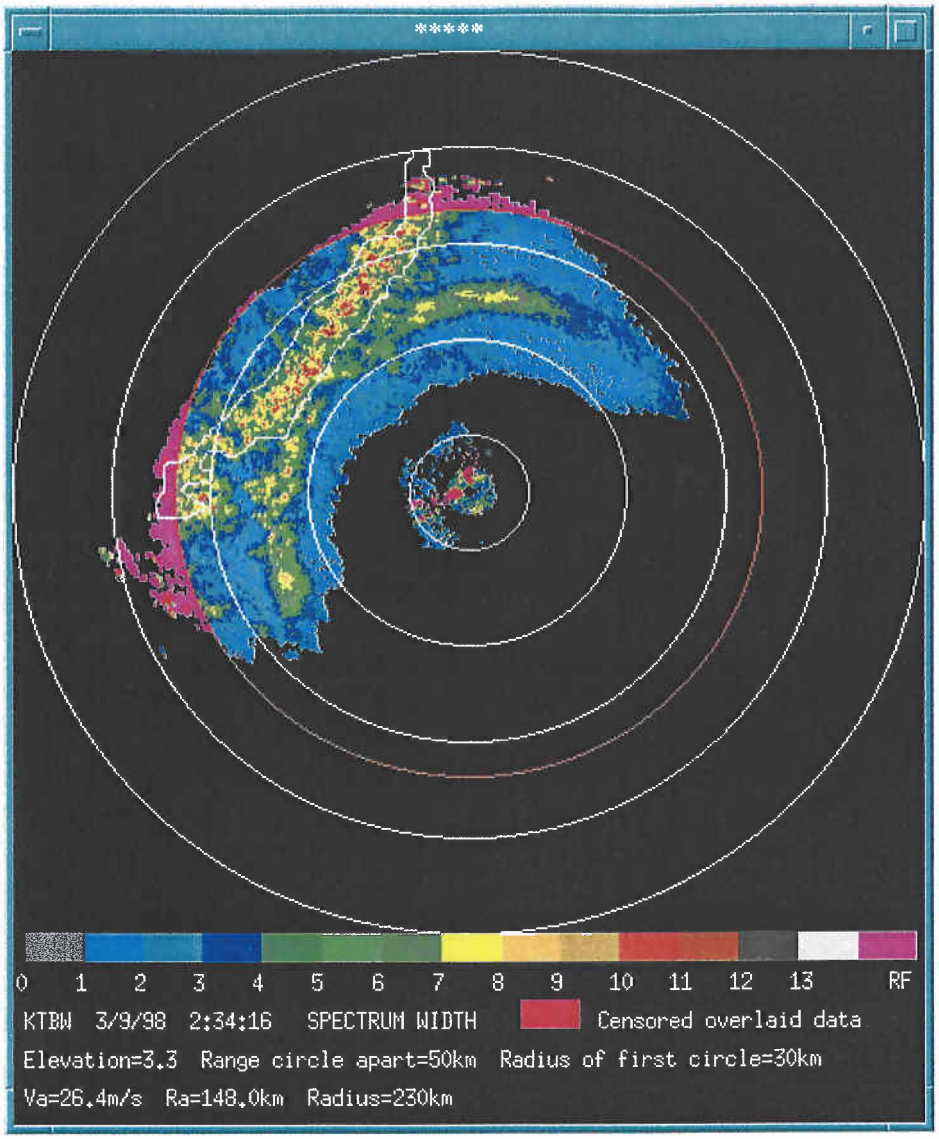

Fig. 8d The spectrum width field associated with Fig. 8c, but at an elevation angle of 3.3°. Note the ring of enhanced spectrum width values at the constant range of 100 km. This feature suggests a layer of shear and/or turbulence at an altitude of about 6.3 km. The spectrum width values along the squall line's convective band continue to be large, but take on the appearance of separated convective elements.

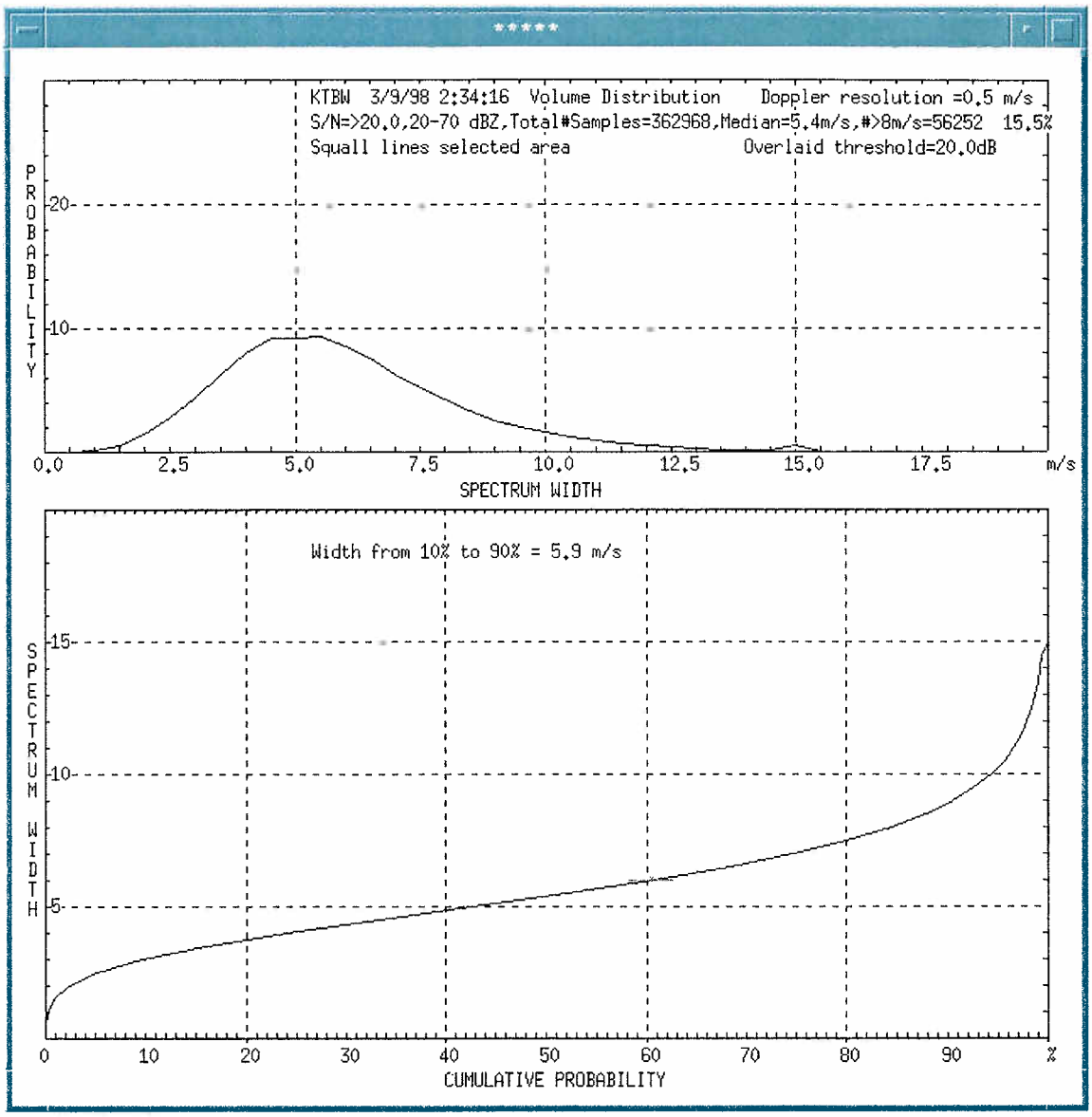

Fig. 8e. The statistics of spectrum width for the portion of the squall line storm enclosed by the white contour in Fig. 8a.

3.7 *Snow*:

These data come from winter conditions for which snow is reported over large areas, and where reflectivity is at least as large as 10 dBZ. Using the accepted Srivastava-Sekhon relation that relates the equivalent rainfall rate R_s of snow to the radar measured equivalent reflectivity factor Z_e, but adjusted for the increase of ice particle volume due to the expansion of ice (Doviak and Zrnic, 1993, Eqs.8.24 and 8.25b),

$$Z_e\,(\mathrm{dBZ}) = 26 + 22.1\,\log_{10}[R_s(\mathrm{mm\ h^{-1}})]\,,$$

where R_s is the equivalent liquid water amount in mm h^{-1} of the snow fall. A simple conversion of equivalent rainfall rate to the depth of snow per hour is obtained by multiplying R_s with 10. Thus a 10 dBZ equivalent reflectivity factor is produced by a snow fall rate that has a corresponding rainfall rate R_s = 0.19 mm h^{-1}; the estimated snow depth rate is about 2 mm h^{-1}, a very light snow fall. So for the most part the lower limit of 10 dBZ should provide us with spectrum width statistics in most regions of significant snowfall. We could have used a smaller lower limit, but judging from the reflectivity fields, the number of data not included is relatively small.

In Fig. 9a is an example of the reflectivity factor field of a snow that fell on east Missouri and west Illinois on the 16th of January, 1994, and was recorded by KLSX WSR-88D radar in Saint Louis, Missouri. The corresponding spectrum width field is presented in Fig.9b, and its statistics are given in Fig. 9c.

The patten of spectrum width field in Fig. 9b is comprised of two semi-circles of enhanced values separated by a region of low widths aligned in a SE to NW direction. This configuration might be the pattern of a shear layer. Regions associated with wind shear can be recognized on the PPI display as two semicircles of enhanced σ_v around the radar at the height where the radar beam intersects the shear layer (Melnikov and Doviak, 2001). Because the beam is at an elevation of 0.5°, the range dependence of spectrum width can also be interpreted as a height dependence, especially if the weather system is vertically stratified as might be expected for snow. If the region of enhanced spectrum width is indeed associated with a shear layer, we can estimate that the layer lies between heights of about 400 and 1100 m. Further analysis is required to support these inferences.

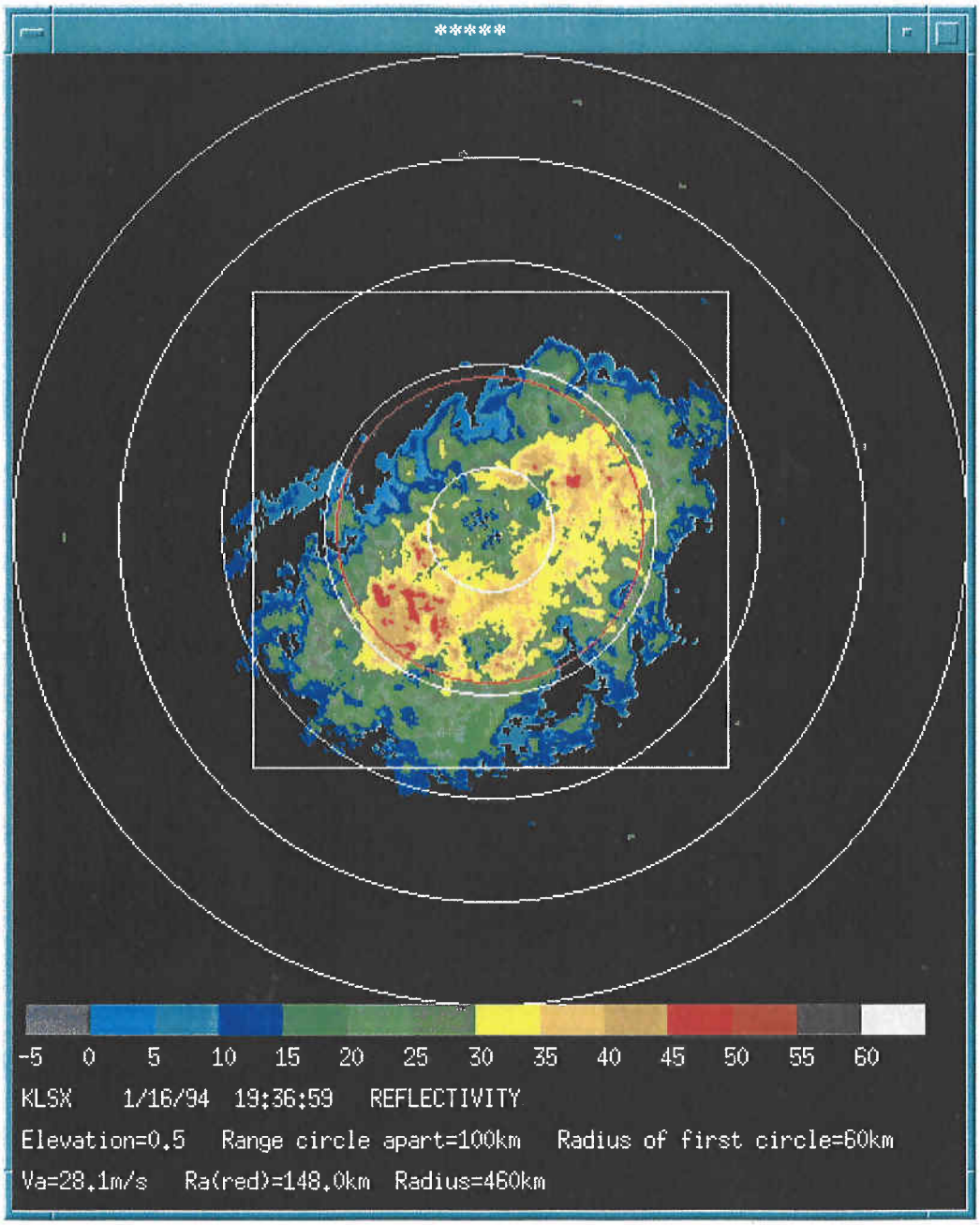

Fig. 9a The reflectivity factor field for a snow storm over St. Louis, MO., on 16 January, 1994 at 19:36.

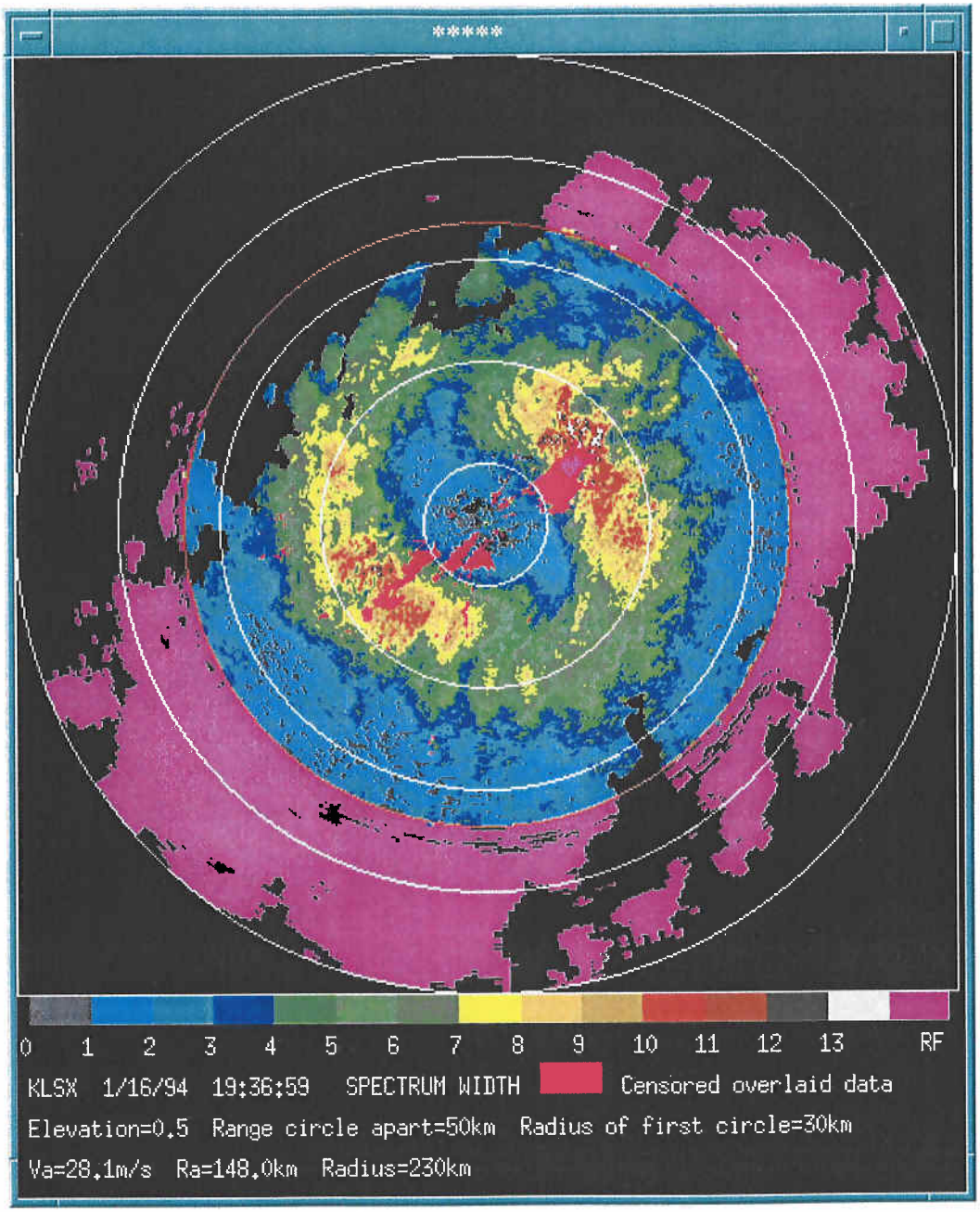

Fig. 9b The spectrum width field for the snow storm having the reflectivity given in Fig. 9a.

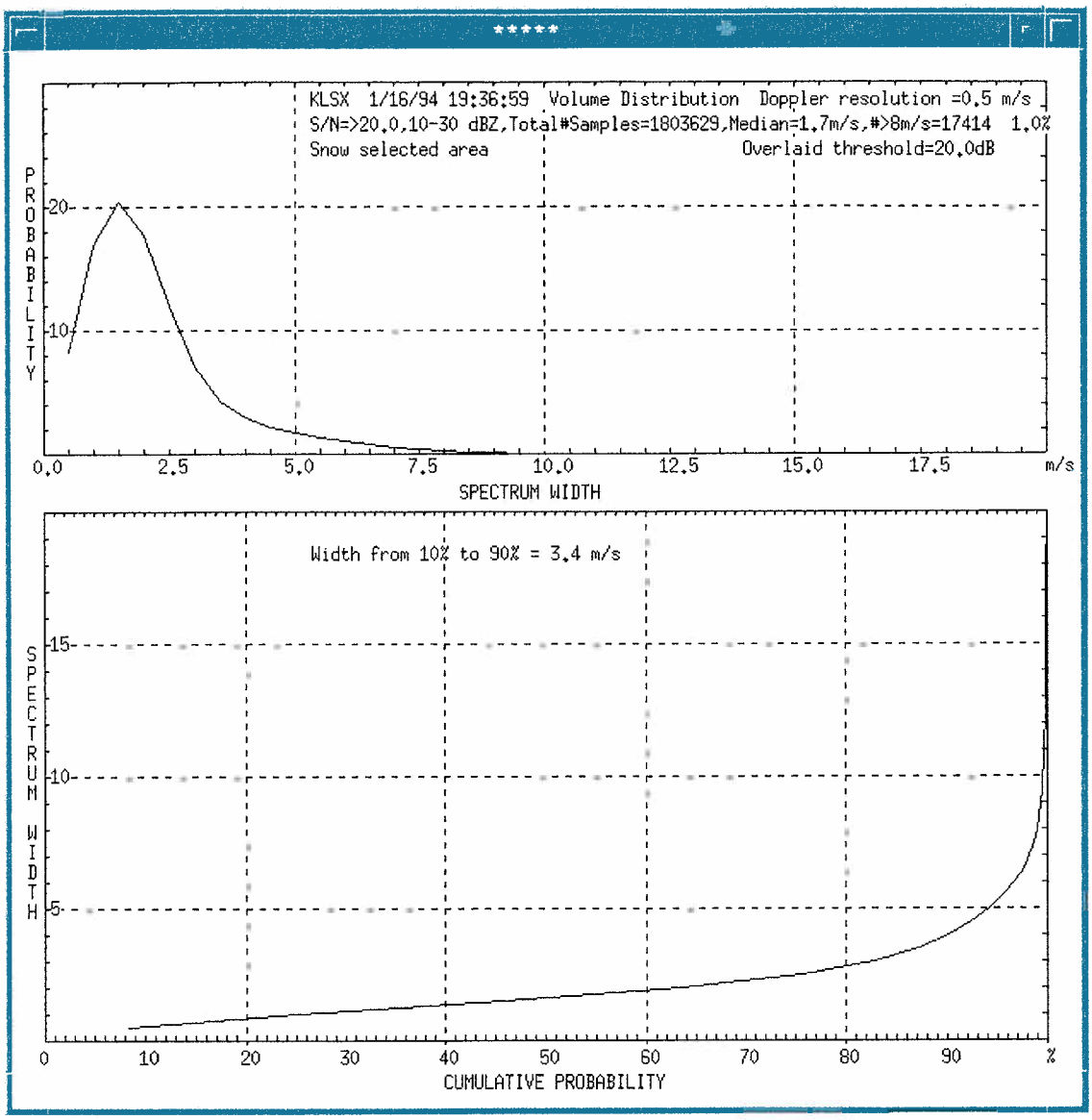

Fig. 9c. The statistics of spectrum width for snow fall.

4. Median spectrum width versus weather class

The median values of spectrum width, for the various weather classes described in the previous section and for the storms analyzed to date, are tabulated in Table 1 in bold type. The Fujita scale "F" rating, indicating the severity of the tornado in the tornadic storms, is listed in this Table. Also listed are the percent of spectrum widths that exceed 8 m s^{-1}. Although the data are limited to one case in some categories, we can make some revealing observations.

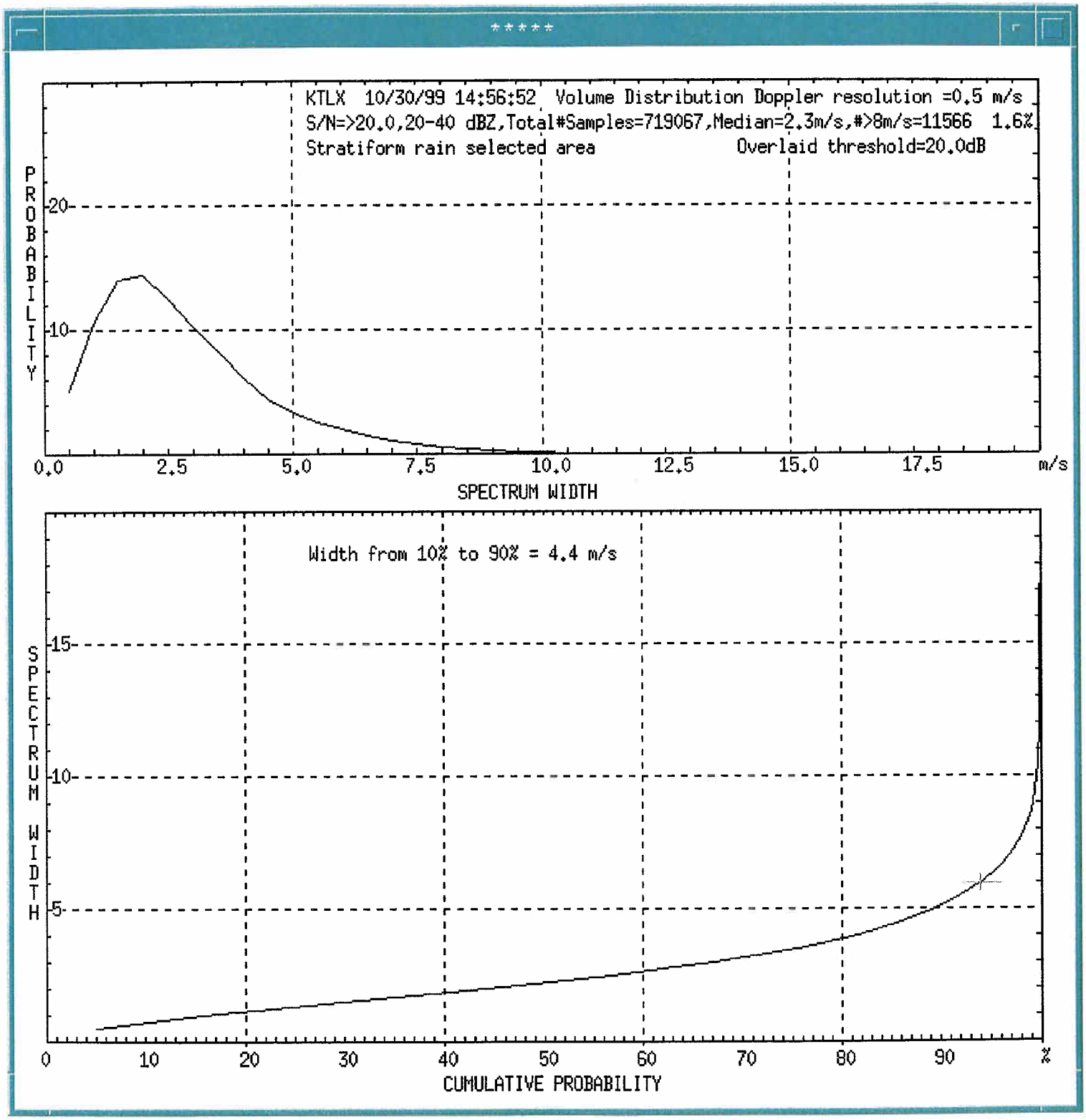
*****
KTLX 10/30/99 14:56:52 Volume Distribution Doppler resolution =0.5 m/s
S/N=>20.0,20-40 dBZ,Total#Samples=719067,Median=2.3m/s,#>8m/s=11566 1.6%
Stratiform rain selected area Overlaid threshold=20.0dB
PROBABILITY
20
10
0.0
2.5
5.0
7.5
10.0
12.5
15.0
17.5
m/s
SPECTRUM WIDTH
Width from 10% to 90% = 4.4 m/s
SPECTRUM WIDTH
15
10
5
0
10
20
30
40
50
60
70
80
90
%
CUMULATIVE PROBABILITY

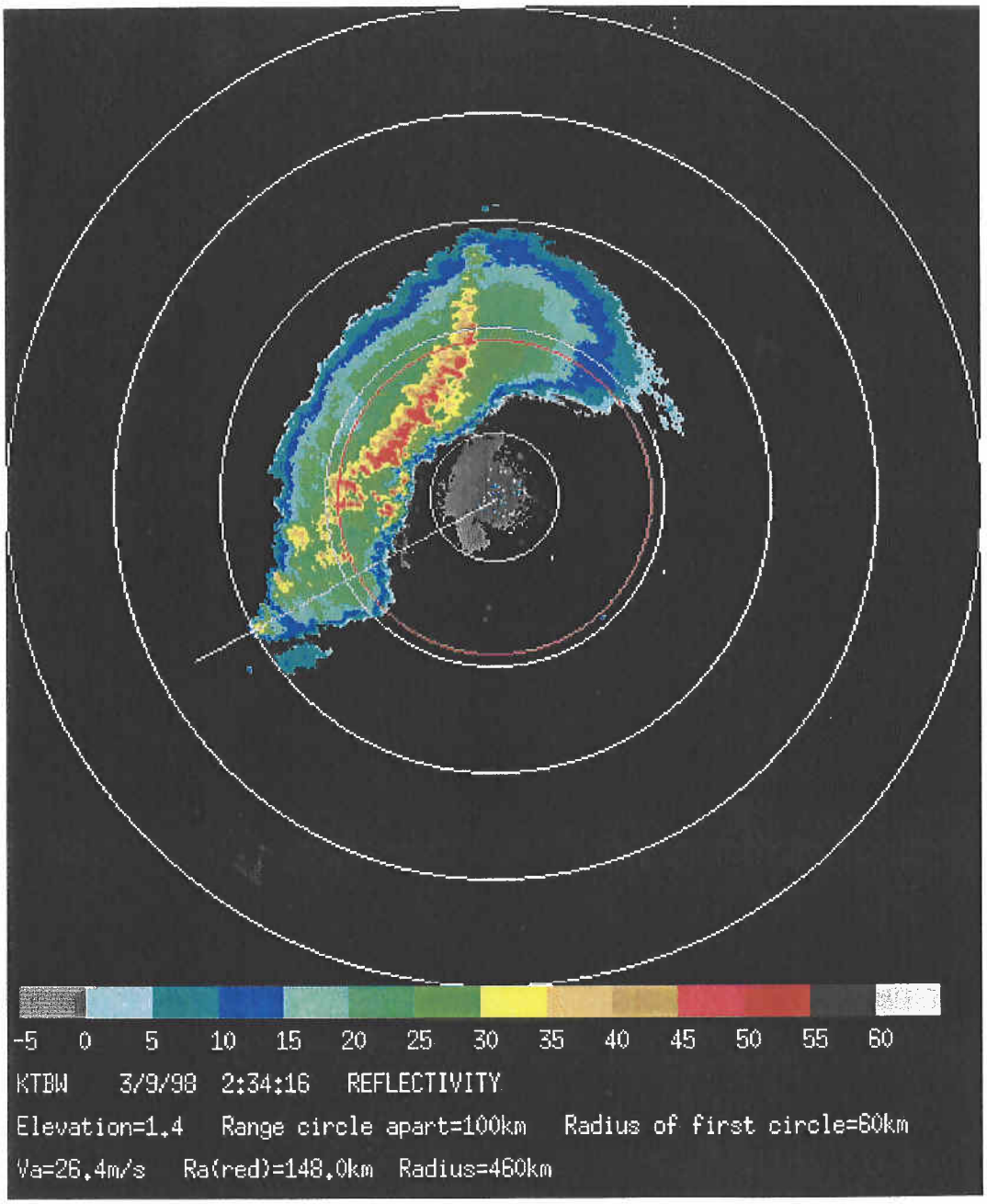
-5 0 5 10 15 20 25 30 35 40 45 50 55 60
KTBW 3/9/98 2:34:16 REFLECTIVITY
Elevation=1.4 Range circle apart=100km Radius of first circle=60km
Va=26.4m/s Ra(red)=148.0km Radius=460km

10.3 km

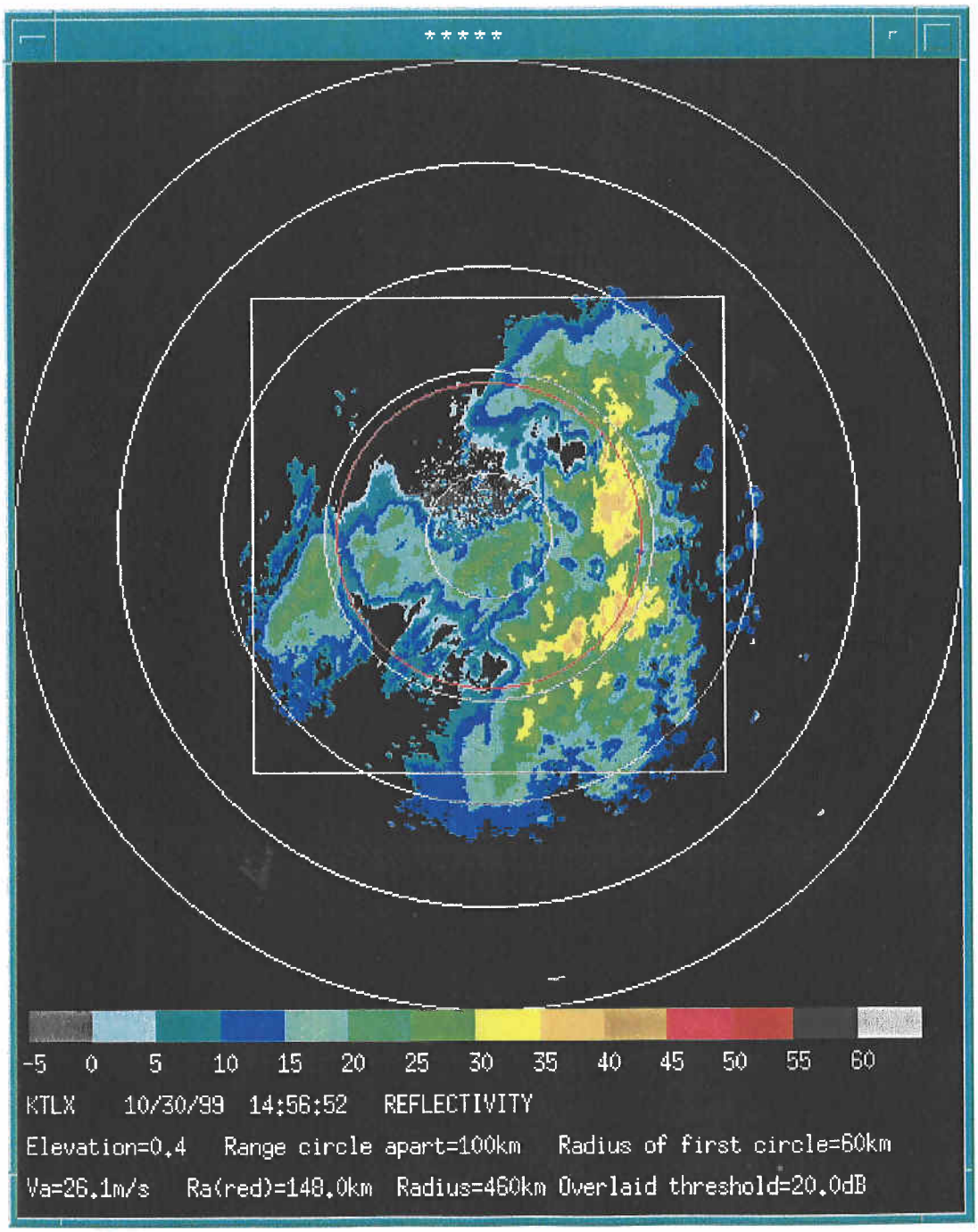

Height ≈ 7 km above ground

Table 2

Median values of spectrum width (m s^{-1}) in single volume scans; and the % larger than 8 m s^{-1}

Clear Air i) 5/13/98 Oklahoma City, OK	(-5≤Z≤10dBZ) **1.9; 0.8%**	**Multi-cell Severe storm** i) 5/3/99 Oklahoma City, OK	(20≤Z≤70 dBZ) **2.9; 3.0%**	
Stratiform rain i) 5/27/95 Des Moines, IA ii) 1/24/97 Nashville, TN iii) 10/30/99 Oklahoma City, OK	(20≤Z≤40 dBZ) **1.5; 0.2%** **1.7; 1.1%** **2.3; 1.6%**	**Squall lines** i) 4/15/94 Saint Louis, MO ii) 3/9/98 Tampa, FL iii) 5/31/98 (1st) iv) 5/31/98 (2nd) Albany, NY v) 1/23/96 Shreveport, LA	(20≤Z≤70dBZ) **4.1; 7.6%** **5.4; 15.5%** **2.1; 0.1%** **3.1; 1.4%** **2.5; 1.0%**	(Comments): embedded embedded embedded and broken early broken mature broken
Snow i) 1/26/00 Oklahoma City, OK ii) 1/16/94 Saint Louis, MO iii) 1/6/95 Saint Louis, MO	(10≤Z≤30 dBZ) **2.0; 0.0%** **1.7; 1.0%** **1.9; 0.4%**	**Isolated storms** i) 5/3/99 (F5) Oklahoma, City, OK ii) 5/31/96 (F3) Aberdeen, SD iii) 4/16/98 (F3) Nashville, TN	(20≤Z≤70 dBZ) **1.8; 0.6%** **1.4; 0.4%** **1.7; 0,7%**	
Widespread showers i) 3/9/98 Tampa, FL	(20≤Z≤45 dBZ) **2.1; 0.0%**			

5. Discussion

All three tornadic storms listed in Table 1 were producing tornados at the time of the analysis. Thus, their very low median spectrum widths are surprising, particularly for the 5/3/99 storm that devastated Moore, OK with an F5 tornado. Nevertheless, the spectrum widths in the region of the tornado was larger than 8 m s^{-1}, but these occupied a small portion of the total data volume. Median spectrum width values inside the high reflectivity core of the storms is about the same as that outside the core as noted in the previous section. The low median values are in contrast to those for squall lines, multi-cell severe storms, and even widespread showers. This suggests that although these isolated storms were tornadic and formed in environments with strong vertical shear, their flow, at least at the time of the tornado, was much less turbulent than that in other weather systems. Perhaps the relatively isolated locations of the storms allowed them to have a well organized structure that permitted them to last a longtime. This view is consistent with the interpretation that these tornadic storms are steady state supercell thunderstorms.

Supercells interact with the environment in such a way as to organize a steady flow of ascending and descending air within the storm while they propagate either to the left or right of the mean tropospheric wind with a velocity that allows them a steady interaction with the large-scale environment of the storm (Browning, 1982). Perhaps the supercell, in a relatively undisturbed environment, has significantly less turbulence. Lilly (1986) shows that rotating supercell storms are characterized by high helicity, and high helicity suppresses nonlinear energy transfer and turbulence generation. So these "unexpected" low spectrum widths could be evidence of high helicity in supercell storms, which is consistent with Wu's (1990) deduction.

On the other hand, storms to the northwest observed at the same time as the isolated supercell have significantly larger median spectrum width values (3.8 m s^{-1} vs 1.7 m s^{-1}) in the regions of high reflectivity (i.e., > 40 dBZ, Fig. 7c). The median value for all regions of reflectivity larger than 20 dBZ lowers from 3.8 to 2.9 m s^{-1} because of the lower spectrum widths (i.e., median value equal to 2.6 m s^{-1}) in regions of lower reflectivity factor (i.e., between 20 and 40 dBZ) persist over much larger areas. Even the velocity field (Fig.6b) in this region of multi-cell storms exhibits larger spatial variance, thus supporting the larger spectrum width values.

Of course the beam width is larger for the more distance storms and it might be expected that a larger variance of the Doppler velocities within the beam would be observed, and thus spectrum widths would, on average, be larger. But Doviak and Zrnic (1993) showed that there was practically no difference in the spectrum width for a tornadic storm that was three times farther than a closer tornadic storm. Therefore it was suggested that the spectrum widths were due to turbulence whose outer scales were smaller than the radar's resolution volume. If turbulence was isotropic with scales larger than the resolution volume, we could at best expect a weak (i.e., $r^{1/3}$) dependence on range (Doviak and Zrnic, 1993; Eq.10.68). Thus, we conclude that the flow in the multi-cell storms to the northwest are more turbulent because they have less helicity than the isolated storm closer to the radar.

Compared to isolated severe storms, squall lines, multi-cell severe storms, and widespread showers have higher spectrum width values, which suggest that their flows are not as steady and smooth as that in supercells. Thus these three weather classes might have a higher efficiency in transforming large scale kinetic energy into turbulent kinetic energy, and eventually heating the air.

The median value of spectrum width of a multi-cell severe storm, in the region where reflectivity factors range from 40 to 70 dBZ, is larger that than in the region where reflectivity factors range from 20 to 40 dBZ (compare Figs. 7b and 7c). This observation suggests that turbulence inside the storm's core is stronger than in the region outside the core.

The spectrum width of the widespread shower case almost equals that for the broken-line squall line in its early stage (i.e., squall line (iii)). This is consistent with the fact that both of them often form in an environment of weak shear and their cells often behave like ordinary cells.

Isolated super cell storms, stratiform rain, snow, and day time fair weather appear to have the smallest spectrum widths. Excepting the isolated tornadic storm cases, this might be expected because turbulence levels in these weather conditions are expected to be lower. But the spectrum widths for non violent weather could be larger than that which could be accounted for by turbulence; that is, vertical shear of wind could be a major contributor to the observed spectrum widths. The contributions of shear to the observed spectrum widths need to be determined using, for example, the methods of Istok and Doviak (1986) before we can draw conclusions concerning the levels of turbulence in the various weather categories. This type of effort is beyond the aim of the present study, but should be done to relate the spectrum width data to meteorological phenomena, and to turbulence that could affect safety of flight.

The largest spectrum width data (i.e., those that have a median value of 5.4 m s^{-1}) is associated with the high reflectivity region of an embedded areal squall line. But the spectrum width of squall lines span a wide range of median values from about 2.5 to 5.4 m s^{-1}; in some cases more than 15% of the width data exceed 8 m s^{-1}. Squall lines may form in environments in which the vertical shear of the wind is different, and this might cause the differences in the structure of the squall line and the spectrum width medians seen among squall lines. Furthermore, the medians would also be a function of the squall line's stage of development. More detail investigations are necessary to reveal the real physical reasons behind these differences.

6. Some comments on use of spectrum width to measure turbulence

The turbulent kinetic energy dissipation rate ϵ is a parameter that has been related to turbulence that affects aircraft flight (e.g., Trout and Panofsky, 1969), and there has been attempts to relate Doppler spectrum width σ_v to ϵ and turbulence affecting aircraft flight (e.g., Bohne, 1982). But there are many problems with using σ_v to estimate ϵ. For example, it must be assumed that the outer scale or wavelength Λ_o of turbulence is much larger than the radar's resolution volume V_6 dimensions; these are determined by the angular resolution or beamwidth and range resolution.

Satisfying the condition that Λ_o must be larger than the dimensions of V_6 is, for weather radars such as the WSR-88D needing to measure ϵ quantitatively over large distances (e.g., 200 km), a difficult one to satisfy. This is because the beam width at that range is more than 3 km in diameter. To compare this beam width with outer scales Λ_o observed in thunderstorms, it is instructive to note that Sinclair (1974) has determined that Λ_o in a severe storm varies from 150 to about 2000 m. Other investigators (e.g., Rhyne and Steiner, 1964; MacCready, 1964; Reiter, 1970) have shown or suggested that Λ_o may vary from 300 to 800 m, depending on the phenomena and the location of measurement. Therefore, with the exception of observations at ranges close to the radar, the dimensions of V_6 are expected to exceed Λ_o, and thus eddy dissipation rate cannot be computed reliably.

Yet, if the largest dimension of V_6 exceeds Λ_o, the spectrum width due to turbulence σ_t (i.e., that contribution to the measured width σ_v remaining after removal of the shear contribution; Istok and Doviak, 1986), would still be due to turbulence which might affect aircraft flight even if one cannot accurately calculate ϵ. If the beam is horizontal, as with an airborne Doppler radar, and turbulence is horizontally isotropic, the dispersion of radial velocities within V_6 and the change of the mean Doppler velocity from one V_6 to the next is a measure of the head to tail wind changes, and these wind changes can affect aircraft performance. From simultaneous measurements of spectrum widths with two spaced Doppler radars surveying few storms, Lee and Thomas (1989) concluded that Doppler spectrum width is practically independent of viewing angle. Thus, not only might σ_v be usefully related to turbulence that affects safe flight, but so might the spatial change of the mean Doppler velocity from V_6 to V_6. This latter approach has not been investigated extensively, but limited observations show that there is correlation between spectrum width and the spatial variability of mean Doppler velocities, as one might expect.

7. Summary, conclusions, and recommendations

The Doppler spectrum width determines the performance of all estimators of Doppler velocity, polarimetric variables (for polarimetric Doppler radar), and of the newly developed techniques to mitigate the occurrence of range and velocity ambiguities. In order that the radar processors provide accurate measurements, spectrum width values need to be small compared to the unambiguous velocity; this is especially critical for range-velocity mitigation techniques. Furthermore, spectrum width is the basic Doppler moment that relates measurements to turbulence, and accurate estimates of spectrum width is crucial to providing good estimates of turbulence. Yet, operational radars generate spectrum width data fields that often contain anomalously large spectrum widths unrelated to meteorological phenomenon such as turbulence. This preliminary study on the statistics of spectrum width shows the following:

1) To have reliable spectrum width data for analysis, the following data censoring thresholds are recommended:
   i) a 20 dB overlaid threshold,
   ii) reject data sets for that day if there is evidence that large spectrum widths are correlated with large reflectivity values, and
   iii) a 20 dB SNR threshold.

2) Isolated super cells, daytime clear air, stratiform rain, and snow produce weather signals (echoes) that have the smallest spectrum width values. The median spectrum widths for these weather categories appear to be less than about 2 m s^{-1}.

3) The largest spectrum widths, ranging from 3.1 to 5.4 m s^{-1}, are associated with embedded areal squall lines

4) Widespread rain showers and multi-cell severe storms have median spectrum width values (2.1 to 2.9 m s^{-1}) that fall in between the above ranges.

5) The spectrum width of squall lines span a wide range of values from about 2 to almost 6 m s^{-1}, which might be related to the type and the stage of squall lines. Further investigation is required to better characterized the spectrum width statistics of squall lines and to relate them to the various stages of the squall line's formation.

6) The surprisingly smaller than expected spectrum width fields for a large number of weather classes suggest that range-velocity mitigation techniques planned for the WSR-88D might work better than anticipated.

7) Because high helicity suppresses the nonlinear energy transfer and turbulence generation, isolated tornadic storms, at least at the time of tornado formation, have a smaller spectrum width than squall lines, multi-cell severe storms, and widespread showers.

8. Acknowledgments

The research reported herein was partially supported by the Radar Operations Center (ROC) of the National Weather Service, in Norman, Oklahoma. Dr. Larry Cornman, of the Research Applications Program of the National Center for Atmospheric Research has been instrumental in obtaining support for this effort. Support for this research is in response to requirements and funding by the Federal Aviation Administration (FAA). The views expressed are those of the authors and do not necessarily represent the official policy or position of the FAA. We also acknowledge the continued encouragement and comments from Dr. D. S. Zrnic of the National Severe Storms Laboratory; and the scientific and technical support of Dr. Valery Melnikov who has shown a keen interest in the spectrum width measurements with weather radars, and who has supplied a steady stream of helpful comments during this project.

9. References

Bluestein, H. B., 1993: Synoptic-Dynamic Meteorology in Midlatitudes, Volume II, Oxford University Press, Oxford, New York. 520-526.

Bohne, A. K., 1982: Radar detection of turbulence severity in precipitation environments. *J. Atmos. Sci.* **39**, 1819-1837.

Browning, K. A., 1982: General circulation of middle-latitude thunderstorms. *In "A Social, Scientific, and Technological Documentary"* (E. Kessler, ed.), Vol. 2, pp. 211-247. NOAA, U.S. Dept. of Commerce. U.S. Govt. Printing Office, Washington, D.C.

Cornman, L. B., R. K. Goodrich, R. Frehlich, B. Sharman, and N. Beagley, 1999: The detection of convective turbulence from airborne Doppler radar. *Preprints, 29th Conf. On Radar Meteorol.,* Montreal, Amer. Meteorol. Soc., Boston. 864-867.

Doviak, R. J., and D. S. Zrnic, 1993: *Doppler radar and weather observations*. Academic Press, Inc., San Diego, CA., 562 pp.

Federal Aviation Administration, 1978: 'Thunderstorms'. Advisory Circular 00-24A, FAA, Department of Transportation, Washington, D. C., 10 pp.

Istok, M. J., and R. J. Doviak, 1986: Analysis of the relation between Doppler spectrum width and thunderstorm turbulence. *J. Atmos. Sci.* **43**, 2199-2214.

Lemon, L. R., 1999: Operational uses of velocity spectrum width data. *Preprints, 29th Conf. On Radar Meteorol.,* Montreal, Amer. Meteorol. Soc., Boston. 776-779.

Lee, J. T., 1977: Application of Doppler radar to turbulence measurements which affect aircraft, Final Rept. No. FAA-RD-77-145. FAA Syst. Res. Dev. Serv., Washington, D. C.

Lee, J. T. and K. Thomas, 1989: Turbulence spectral widths view angle independence as observed with Doppler radar. Technical Rept., DOT/FAA/SA-89-2. 47 pp.

Lilly, D. K., 1986: The structure, energetics, and propagation of rotating convective storms. II, Helicity and storm stabilization. *J. Atmos. Sci.* **43**, 126-140.

MacCready, P. B., Jr., 1964: Standardization of gustiness values from aircraft. *J. Appl. Meteorol.* **3**, 439-449.

Mahapatra, P., 1999: *Aviation weather surveillance systems*. The IEE, 458 pp.

Melnikov, V. M., and R. J. Doviak, 2001: Spectrum widths from echo power differences reveal meteorological features. J. Atmos. and Oceanic Technology; manuscript accepted for publication.

NEXRAD Technical Requirements, 1991: Report #R400-SP401A, November. Copies available from the NEXRAD Joint System Program Office, Silver Spring, MD, 20910, 190 pp.

Rhyne, R. H., and Steiner, R., 1964: Power spectral measurements of atmospheric turbulence in severe storms and cumulus clouds. *NASA Tech. Note* NASA TD D-2469, 1- 48.

Reiter, E. R., 1970: Recent advances in the study of clear air turbulence (CAT). *Rev. Meteorol. Aeronaut.* **30**, 10=13.

Sachidananda, M., 1998: Signal Design and Processing Techniques for WSR-88D Ambiguity Resolution, Part II, 105 pp.

Sachidananda, M., 1999: Signal Design and Processing Techniques for WSR-88D Ambiguity Resolution, Part III, 81 pp.

Sinclair, P. C., 1974: Severe storm turbulent energy structure. *Conf. Aerosp. Aeronaut. Meteorol., 6th, 1974*, El Paso, Texas.

Sirmans, D, R. Gunther, and J. Windes, 1997: Engineering Study of Spectrum Width Anomaly, Informal report submitted to the Operational Support Facility of the National Weather Service, Norman, OK.

Trout, D., and Panofsky, H. A., 1969: Energy dissipation near the tropopause. *Tellus* **21,** 355-358.

Wu. W., 1990: Helical Buoyant Convection. PH.D. Thesis, University of Oklahoma, Norman, OK.

Zahrai, A., J. Carter, V. Melnikov, and I. Ivic, 1998: The Design of a New Signal Processing Subsystem for the WSR-88D (NEXRAD) Radar. !4th International Conference on Interactive Information Processing Systems for Meteorology, Hydrology, and Oceanography. Phoenix,